Research Square

Preprints are preliminary reports that have not undergone peer review.
They should not be considered conclusive, used to inform clinical practice,
or referenced by the media as validated information.

Regulation of schistosomiasis by the host gut microbiome

Thabo Mpotje
International Centre for Genetic Engineering and Biotechnology
Martin Gael Oyono
Ministry of Scientific Research and Innovation
Leonel Meyo Kamguia
Ministry of Scientific Research and Innovation
Mireille Kameni
Ministry of Scientific Research and Innovation
Leonel Javeres Mbah Ntepe
Ministry of Scientific Research and Innovation
Moise Wokam
Ministry of Scientific Research and Innovation
Bernard Marie Zambo Bitye
Ministry of Scientific Research and Innovation
Vanessa Ornella Alactio Tangueu
Ministry of Scientific Research and Innovation
Severin Donald Kamdem
International Centre for Genetic Engineering and Biotechnology
Paballo Mosala
University of Cape Town
Nada Abdel Aziz
International Centre for Genetic Engineering and Biotechnology
Donald D. Nyangahu
University of Cape Town
Fungai Musaigwa
University of Pennsylvania
Erve Martial Kuemkon
Catholic University of Central Africa
Francis Konhawa
Catholic University of Central Africa
Gladys K. Tchanana
Catholic University of Central Africa
Frungwa Nche

University of Yaoundé I

Alim Oumarou
Ministry of Public Health

René Ghislain Essomba
Catholic University of Central Africa

Michel Kengne
Catholic University of Central Africa

Marie Claire Okomo Assoumou
Ministry of Public Health

Katie Lennard
University of Cape Town

Claudia Demarta-Gatsi
Merck (Germany)

Thomas Spangenberg
Merck (Germany)

Frank Brombacher
International Centre for Genetic Engineering and Biotechnology

Justin Komguep Nono
justkoms@yahoo.fr

Ministry of Scientific Research and Innovation

Research Article

Keywords: Schistosomiasis, Gut microbiome, Biomarkers, Fecal microbiota transfer, Purine metabolism

Posted Date: August 14th, 2026

DOI: https://doi.org/10.21203/rs.3.rs-8904686/v1

License: This work is licensed under a Creative Commons Attribution 4.0 International License.
Read Full License

Additional Declarations: Competing interest reported. The authors, through the present, hereby declare that authors TS and CD-G were employed by the company Ares Trading S.A., a subsidiary of Merck KGaA, Darmstadt, Germany during the present study. All remaining authors attested that the research was conducted in the absence of any commercial or financial relationships that could be construed as a potential conflict of interest.

Regulation of schistosomiasis by the host gut microbiome

Thabo Mpotje,[1,2,3,*] Martin Gael Oyono,[4,*] Leonel Meyo Kamguia,[4,5,*] Mireille Kameni,[4,6] Leonel Javeres Mbah Ntepe,[4] Moise Wokam,[4] Bernard Marie Zambo Bitye,[4] Vanessa Ornella Alactio Tangueu,[4] Severin Donald Kamdem,[1] Paballo Mosala,[1,2] Nada Abdel Aziz,[1,2,7] Donald D. Nyangahu,[2,8,9] Fungai Musaigwa,[1,2,10] Erve Martial Kuemkon[11], Francis Konhawa[11], Gladys K. Tchanana[11], Frungwa Nche[12], Alim Oumarou[13], René Ghislain Essomba[11,12,13], Michel Kengne[11], Marie Claire Okomo Assoumou,[13] Katie Lennard,[14] Claudia Demarta-Gatsi[15], Thomas Spangenberg[15], Frank Brombacher,[1,2] Justin Komguep Nono,[2,4,#]

[1]Cytokines and Diseases Group, International Centre for Genetic Engineering and Biotechnology, Cape Town Component, Cape Town, South Africa.
[2]Division of Immunology, Health Science Faculty, University of Cape Town, Cape Town, South Africa.
[3]Africa Health Research Institute, Durban, Kwazulu-Natal, South Africa.
[4]Institute of Medical Research and Medicinal Plant Studies (IMPM), Ministry of Scientific Research and Innovation, Yaoundé, Cameroon.
[5]Ecole Doctorale Régionale (EDR) d'Afrique Centrale en Infectiologie Tropicale, Université des Sciences et Techniques de Masuku (USTM), Franceville, Gabon.
[6]Department of Microbiology and Parasitology, University of Bamenda, Bamenda, Cameroon
[7]Immuno-Biotechnology Group, Biotechnology Department, Faculty of Science, Cairo University, Cairo, Egypt.
[8]Center for Advanced Biotechnology and Medicine, Rutgers University, Piscataway, NJ, USA
[9]Department of Human Pathology, Egerton University, Nakuru, Kenya.
[10]Department of Pathobiology, School of Veterinary Medicine, University of Pennsylvania, Philadelphia, Pennsylvania, United States of America.
[11]School of Health Sciences, Catholic University of Central Africa, Yaoundé, Cameroon
[12]Faculty of medicine and biomedical sciences, University of Yaoundé 1, Yaoundé, Cameroon
[13]Ministry of Public health, Yaoundé, Cameroon
[14]Department of Integrated Biomedical Sciences, Division of Chemical and Systems Biology, Faculty of Health Sciences, University of Cape Town, Cape Town, South Africa.
[15]Global Health R&D of the healthcare business of Merck KGaA, Darmstadt, Germany; Ares Trading S.A. (an affiliate of Merck KGaA, Darmstadt, Germany), Eysins, Switzerland.

* These authors contributed equally

Correspondence: justkoms@yahoo.fr

ABSTRACT

Background: Host responses to helminth infections, such as schistosomiasis, are influenced by genetic factors and the microbiome, which play crucial roles in shaping immune response. This study investigates the interplay between host genetics and the gut microbiome during chronic schistosomiasis.

Results: Using two genetically different murine models (SPF1 C57BL/6 and SPF2 C57BL/6), with different susceptibility to chronic schistosomiasis, we found that the gut microbial profile is vital for the host resistance. Fecal microbiota transfer from the resistant SPF1 C57BL/6 strain to the susceptible SPF2 C57BL/6 strain reduced key pathological features and extended survival. In humans, shotgun metagenomics sequencing and qPCR analysis of stool DNA from school-aged children in *S. mansoni*-endemic areas revealed significant and consensual alterations in gut microbiome composition of schistosomiasis-affected individuals. Notably, we identified two gut bacterial species as reliable biomarkers of schistosomiasis: *Bacteroides ovatus* negatively associated with *S. mansoni* infection, and *Turicibacter sanguinis* correlated positively with liver fibrosis. Multi-omics integration analysis links these bacterial species to distinct altered metabolic pathways, especially the heavy solicitation by both of the purine metabolism and signaling pathway, aligning with the known dependence on the salvage pathway of the *de novo* synthesis of purines by schistosomes during the infection of human hosts.

Conclusion Overall, our findings position the gut microbiome as both determinant of schistosomiasis outcomes and a promising source of biomarkers for the monitoring of infection and morbidity.

Keywords: Schistosomiasis, Gut microbiome, Biomarkers, Fecal microbiota transfer, Purine metabolism

BACKGROUND

Schistosomiasis, caused by trematode worms known as *Schistosoma* [1], affects over 250 million people worldwide, 90% of whom in Africa [2, 3], and leads to more than 200 000 deaths annually [2, 3]. The disease caused by *Schistosoma mansoni* is, in majority of cases, associated with hepato-intestinal inflammation and fibrosis [1]. In severe cases, it can evolve to portal hypertension which can result in death if not treated [1]. A key feature of the pathophysiology is the host immune-driven granulomatous inflammation that develops around the parasite eggs lodged in host tissues. As the infection persists, the inflammatory response becomes modulated, leading to the chronic phase characterized by a state of hypo responsiveness as well as reduced granulomatous immunopathology [4-6]. Inadequate regulation of immune responsiveness and pathological cellular infiltration over time might exacerbate granulomatous inflammation and cause tissue damage [4-7]. This poorly regulated process can further culminate in tissue destruction and impaired organ function [4-7]. Although not necessarily sequential, these pathological processes collectively lead to tissue destruction in infected hosts, a progression that current control tools still fail to adequately monitor [8] and manage[9].

In recent years, host gut microbiota has been identified as an important factor influencing the progression of numerous infectious diseases [10] such as schistosomiasis. A seminal

study by Holzscheiter *et al* [11] demonstrated that administration of a broad-spectrum antibiotic cocktail to reduce gut bacteria resulted in reduced intestinal granulomatous inflammation during *S. mansoni* infection in mice. This suggested that the commensal bacteria could act as regulators of the host pathological response during schistosomiasis. In fact, Osakunor *et al*., [12] revealed specific gut microbiome changes in preschool-aged children (1–5 years) infected with *S. haematobium* in Zimbabwe. *S. japonicum* infection was reported to be associated with specific gut microbiota changes as well, that robustly prevailed in infected individuals[13]. However, the specifics of the contribution of the microbiome to the pathological processes of schistosomiasis are still superficially appraised until date. We indeed noted that all current studies on the gut microbiota signatures during human schistosomiasis are quite limited in the inclusion of true negative controls (i.e. infection controls that do not excrete eggs and morbidity controls that do not present with tissue fibrogranulomatous sequelae among individuals living in the same parasite-endemic areas), conducted with poorly matched cases versus controls and poorly functional in their designs[14-16]. Consequently, further evidence is required to better define the role of the gut microbiota during schistosomiasis both at the infection and disease levels [15].

In this study, we aimed to address such a role of the host gut microbiome during schistosomiasis using:

i- experimental chronic infections of mice i.e. with different genetic make-ups and levels of susceptibility to the disease to functionally assess, by fecal microbiota transfer by cohousing, the role of the gut microbiota in the progression of chronic schistosomiasis-associated fibrogranulomatous disease despite different genetic backgrounds, and

ii- shotgun metagenomics screening of stool DNA from school-aged children from *S. mansoni* endemic areas followed by validation of identified candidate microbial species by qPCR and multi-omics integration to identify consensus microbial and metabolite signatures that might associate, beyond host genetic differences, with *S. mansoni*-infection and/or associated liver pathology.

METHODS

Ethics statement.

i) Mouse studies

Authorization to conduct experiments on animals was granted by the University of Cape Town Animal Ethics Committee (AEC Protocols no. 016/027 and 018/029). All animal experiments were performed to minimize animal suffering in accordance with the guidelines of the Animal Research Ethics committee of the Faculty of Health Science of the University of Cape Town, the South African Veterinary Council (SAVC) and the South African National Standard (SANS 10386:2008).

ii) Human studies

Ethical approval for human studies was granted by the Cameroon National Ethics committee for Human Health Research (Approval no. 2018/02/976/CE/CNERSH/SP). Authorization to conduct the study was also granted by the Ministries of Basic Education (Approval no. 3/105/L/MINEDUB/DREB-C/SDAG/IMS) and Public Health of Cameroon (Approval no. 030-571/L/MINSANTE/SG/DROS/CRC/NPN/TMC/ 631–12.18). The study was conducted with authorization from local, regional and school authorities. Children and parents'/legal guardians were informed of the objectives and the methodology of the study

with assistance from schoolteachers. Participation was voluntary and all children and parents/legal guardians gave informed written consent prior to the study. All collected data were de-identified before downstream analyses to ensure the confidentiality of the participating school children. All school children from the enrolled schools, participant or not, were treated with PZQ as recommended by the Cameroon National program for the control of Schistosomiasis and Soil-transmitted Helminthiasis, regardless of their parasitological status.

Mouse husbandry and species.

The mice that were used in the study were housed and maintained in specific pathogen free facility using ventilated cages containing sterile wood shavings for bedding, in Bio-Safety level 2 (BSL2) facility of the University of Cape Town. Each cage was housing a maximum of 8 mice. The experimental work was conducted according to the recommendations from the University of Cape Town and South African national guidelines for use of procedures for handling of laboratory animals. All efforts were performed to reduce suffering on the animals. A total of 110 wildtype C57BL/6N mice and 110 wildtype C57BL/6J mice were maintained in BSL2 facility and used for the experiments. A sample size of 10 mice per group was utilized in each experiment with a percentage power of 95% and an effect size of 2.5 using a one tail t test. These were to potentially detect with confidence a difference between two independent means that will provide a significance level of $p < 0.05$ as calculated using a statistical tool called G. power 3.0.10 (Franz Faul, Universitat Kiel, Germany). Each experiment included both male and female mice aging between 7 and 10 weeks, and the animals were sex and age

matched across each group of interest using an initial body weight of approximately 15 grams. Furthermore, the animals were subjected to the same food source containing a similar diet with a decontaminated water source.

Maintenance of *S. mansoni* life cycle.

The S*. mansoni* parasites were maintained and grown using both *Biomphalaria glabrata* snails and the BALB/c female mice which were monitored in a Bio-Safety level 2 facility, University of Cape Town.

Co-housing protocol for FMT

Fecal microbiota transfer (FMT) was established by co-housing 10 wildtype C57BL/6N mice with 10 wildtype C57BL/6J mice for a total number of 8 mice per cage at a 1:1 ratio. The cohorts included 6- to 7-week-old male and female mice, with C57BL/6N mice sourced from the SPF1 facility (referred to as SPF1 C57BL/6 mice) and age- and sex-matched C57BL/6J mice from the SPF2 facility (referred to as SPF2 C57BL/6 mice). The mice were co-housed for 7 days prior to *S. mansoni* infection to ensure effective microbiota exchange via coprophagy, as previously established[17]. Chronic schistosomiasis was then induced by infecting the mice percutaneously with a dose of 35 *S. mansoni* cercariae.

Chronic *S. mansoni infection*

In the first series of experimental chronic schistosomiasis tests, a total of 20 wildtype C57BL/6N mice versus 20 wildtype C57BL/6J mice were used for chronic mortality study.

These are two different rooms within the same animal unit where animals are bred prior to transfer to the similar experimental room in BSL2 where acclimatization and infections take place. Practically, for chronic mortality studies, the mice were infected percutaneously with a low dose of 35 *S. mansoni* cercariae to establish a chronic infection of Schistosomiasis which occurs from week 10 post infection. Mice were sex and age matched in each independent experiment. The experimental endpoint was characterized by mice showing body weight loss of up to 20% of the original body weight, or physical impairments resulting in irreversible loss of grip force and motility. Each animal was subcutaneously administered an anesthetic cocktail prior to infestation by live *S. mansoni* infection. The cocktail comprised ketamine (100 mg/ml; 1.2 ml) and xylazine (10 mg/ml; 0.8 ml), diluted in 1× PBS. All procedures were performed in accordance with approved standard protocols under the supervision of a qualified veterinary specialist. Animals were euthanized via halothane gas exposure in a closed chamber for 5 minutes. Death was subsequently confirmed by cervical dislocation prior to downstream procedures.

Egg burden quantification in mice.

The parasite burden from each mouse was calculated by quantifying the number of eggs present in liver tissue affected by the *S. mansoni* parasites as follows; each tissue sample (liver) was first weighed and recorded prior to processing. The samples were then transferred into 15 mL falcon tubes containing 5 mL of 5% potassium hydroxide (KOH) and incubated at 37°C incubator overnight. The samples were then centrifuged for 10 minutes at 2000 rpm and 3 mL of the supernatant was discarded to ensure a total volume of 2ml remained in each tube. The samples were then re-suspended by vortex. An aliquot

of 50µl was used to calculate the number of *S. mansoni* eggs present in each sample using an inverted microscope. The total number of eggs in each sample was then calculated to determine the egg burden.

Histological analysis.

The liver samples were placed in neutral buffered formalin solution to fix them and were then processed. About 5µm sections were stained with hematoxylin and eosin (H&E) or Chromotrope aniline blue (CAB) staining. The diameters of each granuloma that had a single egg were quantified using a morphometry analysis program. The egg diameter was subtracted from the diameter of the whole granuloma. A total of 100 granulomas per group of mice were measured for analysis.

Human observational study design.

A cross-sectional study was conducted in five public schools in the vicinity of a *S. mansoni* infested rivers in 5 different villages namely Yoro 1, Yoro 2, Bongando, Ediolomo and Kedia in Bokito, a rural town located about 100 km from Yaoundé, the capital of Cameroon. This study area and the surveyed *Maquisard* cohort have been previously described [18]. A total of 1002 children were initially recruited in the *Maquisard* cohort and thereafter selection was enforced based on the exclusion of those infected with malaria, hepatitis B/C and other geohelminths. Parasitological and pathological features of *S. mansoni* infection were determined by Kato Katz and ultrasonography, respectively, as previously described [18]. Four clusters were defined based on the presence or absence of *S. mansoni* infection and the presence/absence of liver fibrosis as a proxy for pathology

i.e. SAC presenting with *S. mansoni* infection and liver fibrosis (KK+US-), SAC presenting with *S. mansoni* infection but with no signs of liver fibrosis (KK+US-), SAC without *S. mansoni* infection and presenting with liver fibrosis (KK-US+) and SAC without *S. mansoni* infection and with no signs of liver fibrosis (KK-US-). A selection of 10 individuals per cluster was done to ensure age and gender matching from whom stool sample were collected and kept frozen dry in cryotube at -80^{o}C until processing.

Human stool DNA shotgun metagenomics screening and bioinformatics.

A total of 40 stool samples i.e. 10 per cluster were used for DNA isolation as per the manufacturer's instructions (ZymoBIOMICS DNA Miniprep Kit, Zymo Research, CA, USA). DNA samples were validated for quantity (Nanodrop) and integrity (Agarose Gel electrophoresis) prior to shipment to a service provider (Beijing Genomics Institute, HongKong) for library preparation with magnetic beads and shotgun metagenomics sequencing on Illumina HiSeq PE150-Xten at a 30X depth. From the obtained sequences, quality control was performed to filter out low quality sequences and adapter sequences prior to downstream bioinformatics analyses. High quality reads obtained were assembled by MEGAHIT prior to gene prediction and generation of high-quality gene catalogs using MetaGeneMark and CD-hit. These analyses were conducted sequentially at BGI and the University of Cape Town Computational Biology Hub (CBIO). These catalogs are used for Venn analyses to depict the number of overlapping genes of different groups of individuals. Public catalogues including eggNOG (v5.0, KEGG (89.1), BacMet, Card, COG, CAZy, Swiss-Port and NR were used to annotate the gene catalogues. Taxonomy annotation was then performed to define abundance from gene

abundance table and further used for comparative studies on the four groups (difference analyses, barplots, heatmaps, dimension reduction analyses…). Diversity Analysis was then performed, i.e. with regards to richness for alpha and differences between groups for the beta diversity and finally model prediction was performed on the data. Linear Discriminant Analysis (LDA) was used for differential abundance testing (LEfSe (https://huttenhower.sph.harvard.edu/lefse/)[19]. Additional analysis including diversity analyses was performed in R using established microbiome analysis packages (phyloseq, ggplot2). Specifically in the CBIO metagenomics pipeline: Metagenomics raw reads (.fastq format) were quality checked, filtered, adapter-removed and decontaminated, followed by taxonomic profiling with MetaPhlAn2 [20], using the Nextflow-based pipeline https://github.com/kviljoen/YAMP, which was adapted [21] for implementation on the Ilifu cloud computing facility (https://www.ilifu.ac.za/). Differential abundance testing was performed on the Galaxy implementation of LEfSe [19]. All other downstream analyses were performed in R, using the packages phyloseq [22, 23] and custom microbiome-related functions available here: https://gist.github.com/kviljoen/97d36c689c5c9b9c39939c7a100720b9

Bacterial species-specific qPCR optimization.

Bacteria-specific primers and the bacterial housekeeping gene (conservative fragments in bacterial 16S rRNA genes) were designed by PrimerQuest™ Tool. Briefly, genes specific sequences of each bacterial were downloaded from online databases (NCBI GeneBank, Ensembl bacteria, NBRC and RIKEN BCR) and aligned using the multiple sequence alignment (MSA) tool (BioEdit) to obtain a consensus sequence. The latter was

uploaded to PrimerQuest™ Tool to design specific primers. The PCR amplification specificity of the designed primers (single band) was confirmed *In Silico* using BLASTN form NCBI, followed by gradient PCR performed in a 25 µL reaction of OneTaq Quick-Load 2X Master Mix with Standard Buffer (New England Biolabs) containing 0.5 µL of each primer, 2 µL of the template DNA, 12.5 µL of OneTaq Quick-Load 2X Master Mix and 9.5 µL of Nuclease-free water. Thermal cycler parameters were 94°C for 30 seconds, (94°C 15 seconds, 50-55°C 15 seconds and 68°C 15 seconds) x 30 cycles, and final elongation 68°C 5 minutes. PCR product size were confirmed by agarose gel electrophoresis to ensure a single band product per amplification.

Quantitative Polymerase chain reaction

Real-time qPCR was performed using Luna Universal qPCR Master Mix (New England Biolabs). The qPCR mixture consisted at 10µl of Luna Universal qPCR Master mix, 0.5µl forward primer, 0.5µl reverse primer, 1µl of normalized stool DNA and 8µl of Nuclease-free water in 96-well plates with adhesive sealing; a negative control (H_2O as template) was included within every experiment. The quantitative PCR(qPCR) was performed using SYBR Green I on CFX-96 (Bio-Rad) and the amplification conditions were: (1) initial denaturation at 95° for 60 sec; (2) 40 cycles of denaturation at 95° for 15 s, annealing at 53°C for 15s and extension at 68°C for 15s; and Melt Curve (default setting). Primer efficiency was determined using serial dilutions of a template DNA sample. Ct values (cycle threshold) obtained from each dilution were plotted against the logarithm of the dilution factor to generate a standard curve. The slope of this curve was subsequently used to calculate primer efficiency, the acceptable values was ranging from 85% to 110%.

The abundance of each microbial species biomarker was determined and then normalized by the concentration of the 16S reference gene (normalized abundance of target = concentration of the target/concentration of 16S). Changes of relative abundance of each microbial species between clusters were plotted on GraphPad Prism (8.0.1) and statistical differences were determined by unpaired t-test, Kruskal-Wallis test or Mann-Whitney test as relevant using R software.

Metabolomics extraction, detection and data processing

To identify initial candidate biomarkers of schistosomiasis infection and associated liver morbidity, liquid chromatography combined to mass spectrometry (LC-MS) analyses were performed. Firstly, sample were subjected to metabolite extraction by organic reagent precipitation protein method, and quality control (QC) samples were prepared at the same time (by mixing prepared experimental samples), and the extracted samples were tested on the machine. The QC sample obtained was used for the monitoring of the state of the instrument during liquid chromatography (LC 2777C UPLC system, Waters, UK) and mass spectrometry (MS Xevo G2-XS QTOF, Waters UK) (interspersed per 10 test samples in general).

Metabolomics liquid chromatography phase

All chromatographic separations were performed using an ultra-performance liquid chromatography (UPLC) system (Waters, UK). An ACQUITY UPLC HSS T3 column (100mm*2.1mm, 1.8μm, Waters, UK) was used for the reversed phase separation. The column oven was maintained at 50°C. The flow rate was 0.4 ml/min and the mobile phase

consisted of solvent A (water + 0.1% formic acid) and solvent B (methanol + 0.1% formic acid). Gradient elution conditions were set as follows: 0~2 min, 100% phase A; 2~11 min, 0% to 100% B; 11~13 min, 100% B; 13~15 min, 0% to 100%. The injection volume for each sample was 5 μL.

Metabolomics mass spectrometry phase

A high-resolution tandem mass spectrometer Xevo G2 XS QTOF (Waters, UK) was used to detect metabolites eluted form the column. The Q-TOF was operated in both positive and negative ion modes. For Positive ion mode, the capillary and sampling cone voltages were set at 3.0 kV and 40.0 V, respectively. For Negative ion mode, the capillary and sampling cone voltages were set at 2.0 kV and 40.0 V, respectively. The mass spectrometry data were acquired in Centroid MSE mode. The TOF mass range was from 50 to 1200 Da and the scan time was 0.2 s. For the MS/MS detection, all precursors were fragmented using 20-40 eV, and the scan time was 0.2 s. During the acquisition, the LE signal was acquired every 3s to calibrate the mass accuracy. Furthermore, in order to evaluate the stability of the LC-MS during the whole acquisition, a quality control sample (pool of all samples) was acquired after every 10 samples.

Metabolite annotation and analysis

The KEGG database (https://www.genome.jp/kegg/pathway.html), HMDB database (https://hmdb.ca/metabolites), and LIPIDMaps database (http://www.lipidmaps.org/) were used for metabolite annotation. For multivariate analysis, metaX software was used to perform data transformation and subsequently conducted principal component analysis

(PCA) and Partial least squares discrimination analysis (PLS-DA) to classify distinct groups and determine the variable importance in the projection (VIP) associated with each metabolite. In univariate analysis, a t-test was used to determine the statistical significance (P-value) of each metabolite between KK-US- and KK+US- (infection) and between KK+US- and KK+US+ (*S. mansoni*-associated liver fibrosis), while fold change (FC) of each metabolite was calculated. The conditions for screening differential metabolites included Variable Importance in Projection (VIP) scores ≥1.5, Fold Change (FC) ≥1.2 or FC< 0.83 and P-value< 0.05. This approach identified 82 significantly expressed metabolites for non-morbid infections and 33 metabolites for *S. mansoni*-associated liver fibrosis (Figure S1).

Bioinformatics Pipeline

Raw data were processed according to the bioinformatics pipeline step (Figure S1).

AMON tool

AMON tool was used to relate the stool microbiome assessed with shotgun metagenomics sequencing to the plasma metabolome assessed with untargeted LC/MS, in two cohorts namely *S. mansoni* infected school-aged children with liver morbidity (KK+US+) compared to *S. mansoni*-infected SAC without liver morbidity (KK+US-) and the later compared to *S. mansoni*-negative control (KK-US-). AMON tool determined the degree to which annotated compounds in the plasma metabolome of our study cohorts may have been produced by bacteria present in fecal samples, the host, either (i.e. both are capable of production), or neither (i.e. neither the human or the fecal microbiome are

predicted to be capable of producing the observed metabolites)[24], as described herein (Figure S1).

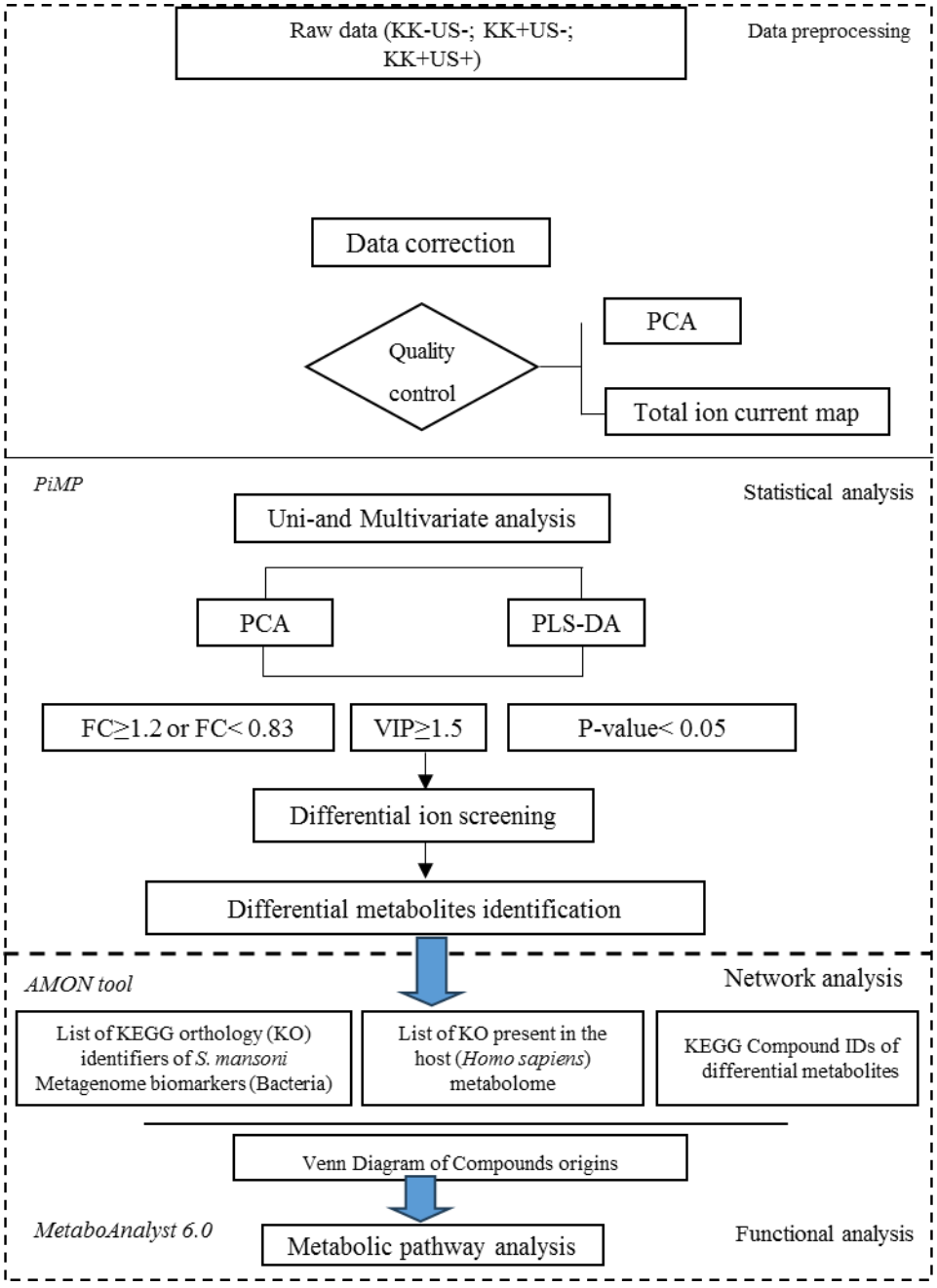


Figure S1. Workflow for cross-cohort integration analysis of fecal metagenomics and plasma metabolomics in *S. mansoni* infected SAC. Figure represents a comprehensive analytical pipeline for integrating metabolomics and metagenomics data to elucidate host-microbe metabolic interactions. The process begins with raw mass spectrometry data (KK-US^{-}, KK^{+}US^{-}, KK^{+}US^{+}) that undergoes preprocessing through xMSanalyzer, including format conversion, noise filtering, peak matching and

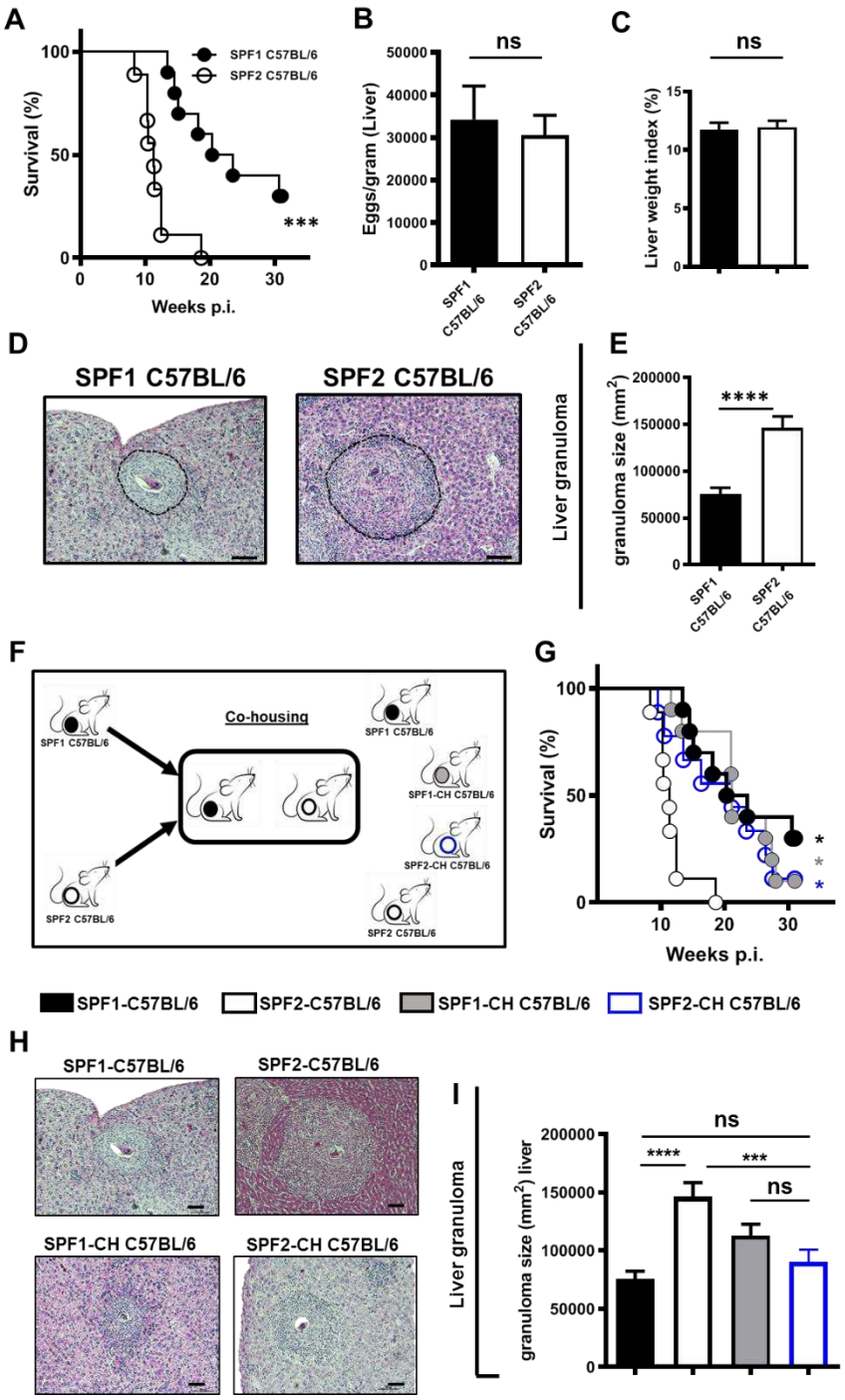
extraction, followed by quality control via PCA and total ion current normalization. Statistical analysis is then performed using Polyomics integrated Metabolomics Pipeline (PiMP), employing both PCA and PLS-DA to identify differential metabolites based on stringent criteria (fold change ≥1.2 or <0.83, VIP≥1.5, and P-value<0.05). The identified differential metabolites are subsequently analyzed using the AMON tool, which integrates three key data sources: KEGG orthology identifiers from identified *Schistosoma mansoni* metagenome biomarkers (bacteria), KEGG orthology identifiers from the Homo sapiens metabolome (host), and KEGG compound IDs of the differential metabolites obtained from LC/MS Untargeted metabolomics. A Venn diagram analysis determines the origin of compounds by comparing metabolite presence across bacterial and host metabolomes, distinguishing which metabolites are uniquely microbial, host-derived, or potentially produced by either organism. Finally, MetaboAnalyst 6.0 performs metabolic pathway analysis to provide functional interpretation, revealing which biological pathways are significantly affected. KEGG organism identifiers:
T06584 tsg; *T. sanguinis* MOL361 (Scheme A- *S. mansoni* related fibrosis); T04113 boa; *B. ovatus* ATCC 8483; T01001 hsa; *Homo sapiens* (human) (Scheme C- *S. mansoni* asymptomatic infection).

RESULTS

Gut microbiota determines chronic schistosomiasis outcomes

To mechanistically explore how the gut microbiome might regulate schistosomiasis and its associated immunopathological responses, mice from 2 genetically distinct breeds[25] were used , i.e. SPF2 C57BL/6 and SPF1 C57BL/6. These animals were percutaneously infected with a low dose of 35 *S. mansoni* cercaria and monitored until they reached experimental endpoint as described in methods sections. An increased susceptibility of the SPF2 C57BL/6 when compared to SPF1 C57BL/6 was observed to chronic schistosomiasis (Figure 1). Specifically, our findings revealed premature mortality among SPF2 C57BL/6 ($P \leq 0.01$) (Figure 1A), despite similar egg burdens in livers (Figure 1B) and comparable hepatomegaly (Figure 1C). This higher susceptibility of SPF2 C57BL/6 was associated with augmented peri-ova granulomatous inflammation in the livers ($P \leq 0.001$) (Figures 1D-E).

Fecal microbiota transfer (FMT) by transient co-housing of a group of susceptible strain (SPF2-CH C57BL/6) with a group of resistant strain (SPF1-CH C57BL/6) prior to chronic schistosomiasis infection (Figure 1F) rescued the susceptible group (SPF2-CH C57BL/6) from premature mortality without increasing susceptibility in the formerly resistant SPF1-CH C57BL/6 animals (Figure 1G). Liver histology revealed a significant reduction of the peri-ova granulomatous inflammation in SPF2-CH C57BL/6 when compared to the non-co-housing SPF2-C57BL/6 (Figure 1H). Notably, SPF1-CH C57BL/6 did not show increased peri-ova inflammation in livers when compared to the resistant non-co-housing SPF1-C57BL/6 (Figure 1I).



406

407 **Figure 1. Transfer of the gut microbiome by transient co-housing with resistant mice rescues**
408 **susceptible mice from chronic schistosomiasis morbidity and mortality.** (**A**) Survival curves of *S.*
409 *mansoni*-infected SPF1 C57BL/6 and SPF2 C57BL/6 mice. SPF1 C57BL/6, n = 10; SPF2 C57BL/6, n = 10.
410 (**B**) Quantification of egg burdens from livers from culled animals during the follow-up. (**C**) Liver weight
411 indexes after death during the 30 weeks follow up. The p-values were determined in B and C using Mann
412 Whitney U test. (**D**) Image scans of H&E-stained liver sections from chronic *S. mansoni*-infected mice (scale

bar = 100 µm). (**E**) Computed measurements of granulomas (mm^2) surrounding trapped *S. mansoni* eggs observed in the liver tissues of chronically infected SPF1 C57BL/6 (n = 10 mice for 100 granulomas measured), and SPF2 C57BL/6 (n = 10 mice for 100 granulomas measured) mice. p-values were determined using the Student's t test. (**F**) Experimental layout for co-housing SPF1 C57BL/6N and SPF2 C57BL/6J mice for 7 days prior to *S. mansoni* infection. This was done by placing mice from each group at a 1:1 ratio in the same cage i.e. 4 x SPF1 C57BL/6 + 4 x SPF2 C57BL/6 into a typical 8-mice cage. The mice were housed together for 7 days to allow enough time for microbial reprograming/acclimatization in each group. This was then followed by a low dose infection of 35 *S. mansoni* infection. (**G**) Survival curve of *S. mansoni*-infected SPF1 C57BL/6, SPF2 C57BL/6, SPF1-CH C57BL/6 (SPF1 C57/BL6 mice co-housed with SPF2 C57/BL6 mice) and SPF2-CH C57BL/6 mice (SPF2 C57/BL6 mice co-housed with SPF1 C57/BL6 mice). SPF1 C57BL/6, n = 10; SPF2 C57BL/6, n = 10; SPF1-CH C57BL/6, n = 10; SPF2-CH C57BL/6J, n = 10. p-values were determined using log-rank test for G. (**H**) Image scans of H&E-stained liver sections from chronic *S. mansoni*-infected mice after the co-housing experiment (scale bar = 100 µm). (**I**) Computed measurements of granulomas (mm^2) surrounding trapped *S. mansoni* eggs observed in the liver tissues of chronically infected mice (n = 10 mice for 100 granulomas measured for each group). p-values were determined using ANOVA followed by Bonferroni correction for multiple comparisons. All figures are representatives from two or more independent experiments with two batches of distinct mouse breeds. Data are presented as means ± SEM. *, p≤0.05; ***, p≤0.01; ****, p≤0.001. ns; non-significant.

S. mansoni-infection and associated liver pathology consensually alters the gut microbiome of school-aged children living in endemic areas

To clinically translate the regulatory role of the gut microbiome in chronic schistosomiasis, as suggested by our preclinical outcomes, we recruited school-aged children (SAC), aged 7 to 16 years old, from the *S. mansoni*-endemic rural areas of Bokito, Cameroon, to undergo a staircase selection procedure of gut microbial typing (Figure 2).

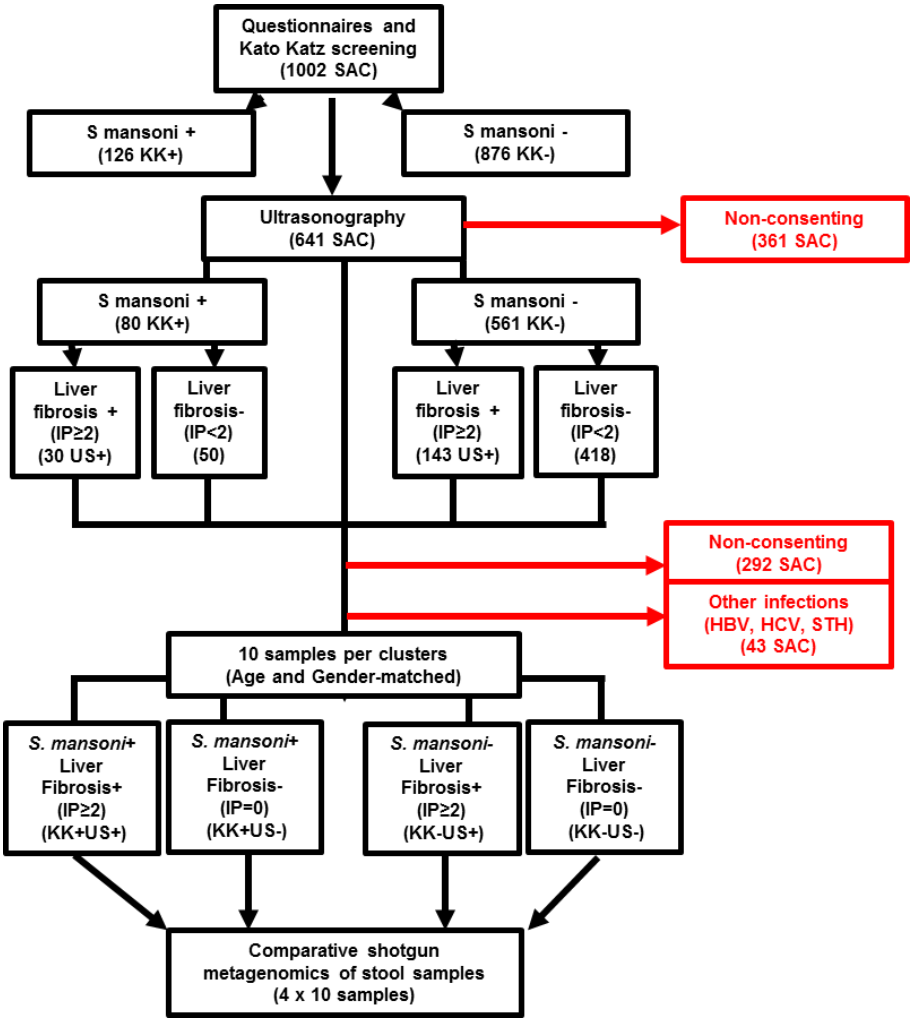


Figure 2: Experimental design of Human Study - the Maquisard cohort. 1002 school-aged children were screened in a rural area of Cameroon centre region endemic for *S. mansoni*. Questionnaires were administered for collection of basic socio-demographical data and stool samples were collected twice over a 5 days period for colposcopy by Kato Katz technique to identify egg-positive participants (KK+) and egg-negative participants (KK-). Abdominal ultrasonography was performed on consenting SAC and classified as presenting with liver fibrosis traits (Image pattern score ≥ 2, i.e. US+) or with no definitive signs of liver fibrosis (Image Pattern score =0). Blood and stool samples from participants further consenting were screened for additional infections such as hepatitis B virus (HBV), hepatitis C virus (HCV) and soil-transmitted helminth (STH) and excluded from the study when found positive for any of these. From the remaining SAC, clusters were classified as presenting with *S. mansoni* eggs in the stools (KK+) or not (KK-) and/or presenting with traits of liver fibrosis (US ≥ 2, i.e. US+) or with no signs of liver image pattern alterations (US=0 i.e. US-) to define 4 clusters i.e. KK+US+, KK+US-, KK-US+ and KK-US-. Ten representative SAC per cluster were selected with similar age and gender distribution across the 4 clusters

and their stool samples were used for DNA isolation and shotgun metagenomics sequencing for comparative assessment of the gut microbial profiles between clusters.

Selected SAC were clustered in groups according to the selection protocol that separated egg-excreting individuals i.e. infected (KK+) from non-excreting individuals i.e. non-infected (KK-). Children were further separated based on liver texture (indicative of liver fibrosis), using an image pattern score and following the WHO Niamey protocol [26] into two sub-groups: (1) Those with altered liver texture (liver fibrosis) who had an image pattern score of at least 2 (US+) or (2) Those without signs of liver fibrosis who had an image pattern score of 0 (US-). Overall, a composite of 4 different clusters defined based on the infectious status (KK+, KK-) and the pathology status (US+, US-) was obtained i.e. KK+US+ (*S. mansoni*-infected and presenting with liver fibrosis), KK+US- (*S. mansoni*-infected and with no signs of liver fibrosis), KK-US+ (*S. mansoni*-egg negative and presenting with liver fibrosis) and KK-US- (*S. mansoni*-egg negative and with no signs of liver fibrosis).

For the discovery phase, a subset of 40 age/gender-matched participants (10 participants per cluster) was selected across the four clusters (Figure 2) and whole genome shotgun metagenomics sequencing of the gut microbial populations was performed for discovery of microbial signatures (Table S1and Supplementary Material 1).

Table S1: **Characteristics of the selected participants for the discovery phase by whole genome shotgun metagenomics sequencing.**

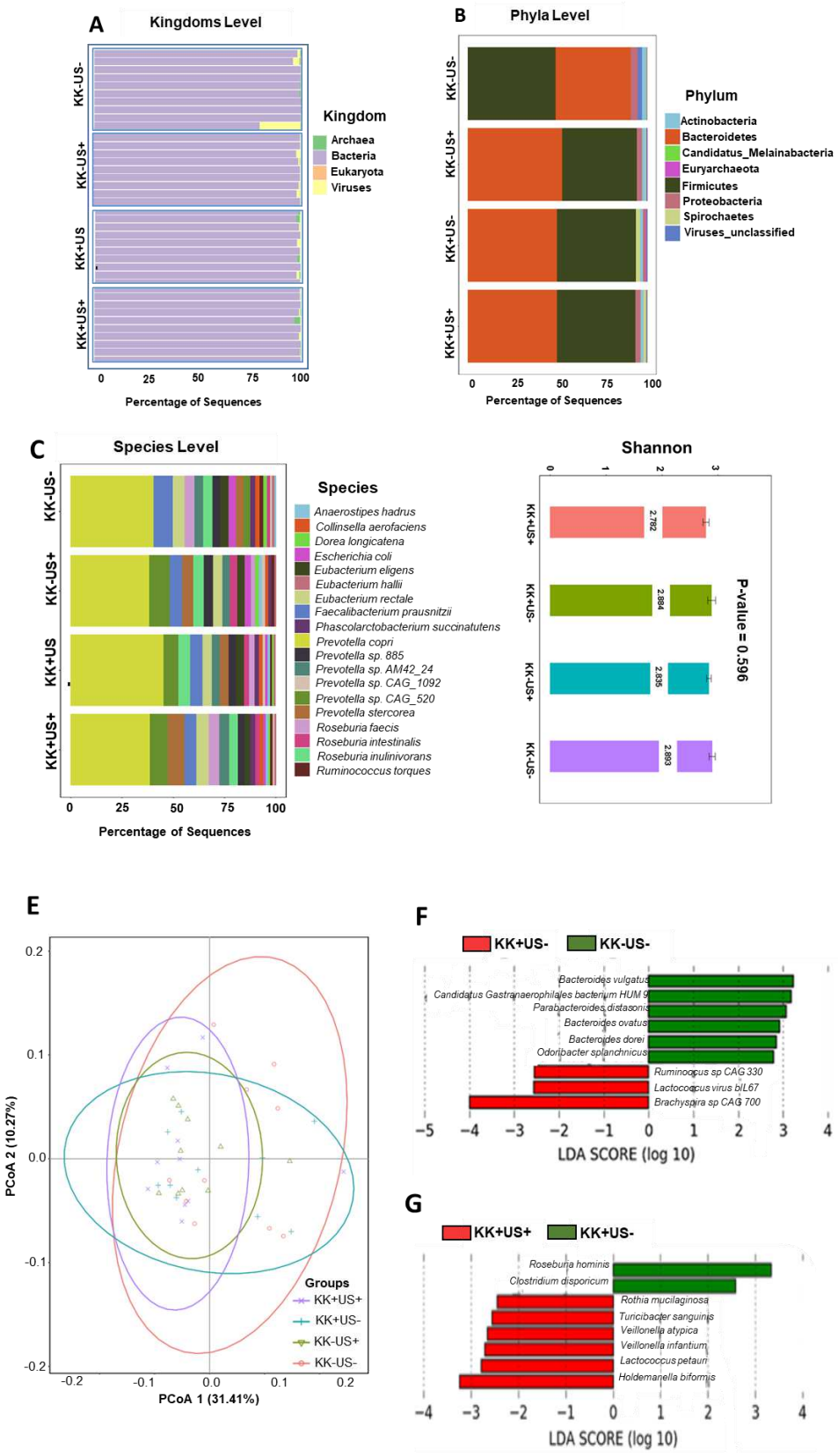
Factors	KK+US+ n=10	KK+ US- (n=10)	KK- US+ (n=10)	KK- US (n=10)	p-values
Age (years) range :	[7-16]	[9-15]	[7-14]	[8-13]	0.35
Mean (SD)	11 (3.16)	11.9 (2.33)	10 (2.21)	10.3 (1.41)	
Sex ratio (Male/Female)	5/5	4/6	7/3	5/5	0.97
BMI	16.47	16.81	15.11	16.21	0.19
Mean (SD)	(1.55)	(1.50)	(1.50)	(1.27)	
Length of residence (years)	6.17	9.00	8.00	4.50	0.70
Mean (SD)	(3.31)	(1.41)	(NA)	(0.70)	
Freq Contact with water/day: Mean (SD)	2.5 (1.50)	1.7 (1.70)	2.2 (1.61)	1.2 (1.47)	0.28
Eggs Burden	36	54	0	0	0.33
Median (range)	(12 -4572)	(12 - 312)	(0)	(0)	
PPF grades					
Possible PPF	06	00	00	00	NA
PPF	04	00	08	00	NA
Advanced PPF	00	00	02	00	NA

KK(+): Kato katz positive (*S. mansoni* eggs-positive); KK(-): Kato Katz negative (*S. mansoni* eggs-negative); US(+): Positive for ultrasonography (clearly defined hepatic fibrosis); US(-): Negative for ultrasonography (No hepatic fibrosis); BMI: Body Mass Index; PPF: Periportal fibrosis; SD: standard deviation; Freq: Frequency; n: number; PPF: Periportal fibrosis; NA: Not applicable.

Metagenomics analyses identified a total of 3490 taxa spanning 4 kingdoms, 42 phyla, 64 classes, 118 orders, 238 families, 710 genera, and 2313 species. Among these, Bacteria were the most represented kingdom across samples (Figure 3A), with Firmicutes and Bacteroidetes emerging as the dominant phyla (Figure 3B). At the species level, the top 10 taxa across the four clinical phenotypes included *Prevotella copri*,

488 *Faecalibacterium prausnitzii*, *Eubacterium rectale*, *Prevotella* sp. CAG_520, *Prevotella*
489 sp. AM42_24, *Prevotella* sp. 885, *Roseburia inulinivorans Prevotella stercorea*,
490 *Roseburia intestinalis* and *Phascolarctobacterium succinatutens* (Figure 3C).

491


A
Kingdoms Level
KK-US-
KK-US+
KK+US
KK+US+
0
25
50
75
100
Percentage of Sequences
Kingdom
Archaea
Bacteria
Eukaryota
Viruses
B
Phyla Level
KK-US-
KK-US+
KK+US-
KK+US+
0
25
50
75
100
Percentage of Sequences
Phylum
Actinobacteria
Bacteroidetes
Candidatus_Melainabacteria
Euryarchaeota
Firmicutes
Proteobacteria
Spirochaetes
Viruses_unclassified
C
Species Level
KK-US-
KK-US+
KK+US
KK+US+
0
25
50
75
100
Percentage of Sequences
Species
Anaerostipes hadrus
Collinsella aerofaciens
Dorea longicatena
Escherichia coli
Eubacterium eligens
Eubacterium hallii
Eubacterium rectale
Faecalibacterium prausnitzii
Phascolarctobacterium succinatutens
Prevotella copri
Prevotella sp. 885
Prevotella sp. AM42_24
Prevotella sp. CAG_1092
Prevotella sp. CAG_520
Prevotella stercorea
Roseburia faecis
Roseburia intestinalis
Roseburia inulinivorans
Ruminococcus torques
Shannon
0
1
2
3
KK+US+
KK+US-
KK+US+
KK-US-
2.782
2.884
2.835
2.893
P-value = 0.596
E
0.2
0.1
0.0
-0.1
-0.2
-0.2
-0.1
0.0
0.1
0.2
PCoA 2 (10.27%)
PCoA 1 (31.41%)
Groups
KK+US+
KK+US-
KK-US+
KK-US-
F
KK+US-
KK-US-
Bacteroides vulgatus
Candidatus Gastranaerophilales bacterium HUM 9
Parabacteroides distasonis
Bacteroides ovatus
Bacteroides dorei
Odoribacter splanchnicus
Ruminococcus sp CAG 330
Lactococcus virus bIL67
Brachyspira sp CAG 700
−5
−4
−3
−2
−1
0
1
2
3
4
LDA SCORE (log 10)
G
KK+US+
KK+US-
Roseburia hominis
Clostridium disporicum
Rothia mucilaginosa
Turicibacter sanguinis
Veillonella atypica
Veillonella infantium
Lactococcus petauri
Holdemanella biformis
−4
−3
−2
−1
0
1
2
3
4
LDA SCORE (log 10)

492

Figure 3: Compositional analysis of the gut microbiome by clinical phenotype in SAC from *S. mansoni*-endemic area. Relative abundance of gut microbial Kingdoms (**A**), Phyla (**B**), and Species level (**C**) among the four clinical phenotypes. Colours of rectangles correspond to the taxa in the legend. (**D**) Alpha diversity (Shannon diversity index) among the four clinical phenotypes at [shown as bar graphs]. (**E**) Principal Coordinates Analysis (PCoA) based on Bray–Curtis distance. Data points in different shapes and colours represent for individuals in different phenotypic clusters. **(F, G**) Linear Discriminant Analysis bar plots showing biomarkers whose LDA scores are greater than pre-set value (default value: 2, $P < 0.05$) between egg-positive cluster (KK+US-) and egg-negative cluster (KK-US-) as determinants of *S. mansoni* infection for (**F**) and Egg-positive & liver fibrosis positive cluster (KK+US+) and Egg-positive & Liver fibrosis negative cluster (KK+US-) as determinants of liver fibrosis during *S. mansoni* infection for (**G**).

Shannon diversity index revealed a modest decrease in microbial diversity at the species level across the four cluster (median values: KK+US+, 2.782; KK+US-,2.884; KK-US+,2.835; KK-US-, 2.893), although the differences were not statistically significant (Figure 3D; $P = 0.596$). In contrast, principal coordinates analysis (PCoA) based on Bray-Curtis distances (Figure 3E, $P = 0.0005$) demonstrated clear clustering of sample into four distinct groups. The greatest divergence was observed between KK+US+ and KK-US- clusters, highlighting pronounced differences in gut microbiome composition between *S. mansoni*-infected individuals with liver fibrosis and uninfected controls. KK+US- and KK-US+ clusters formed distinct yet partially overlapping profiles, potentially reflecting transitional microbial states. Together, these findings support the presence of phenotype-specific microbial signatures.

To deeply explore gut microbial community changes that might occur during infection and/or at the onset of infection-related liver fibrosis, two distinct comparisons were conducted: KK-US- vs KK+US- (Figure 3F) and KK+US- vs KK+US+ (Figure 3G). Linear discriminant effect size analysis (LefSe, Figures 3F & 3G) revealed significant and

biological relevant dissimilarities between clusters *adj P* < 0.05; logFC > 2). Infection-enriched taxa included *Ruminococcus* sp*., Lactococcus virus* and *Brachyspira* sp., while infection-depleted taxa comprised *Bacteroides vulgatus, Candidatus Gastranaeorphilales bacterium, Parabacteroides distasonis, Bacteroides ovatus, Bacteroides dorei* and *Odoribacter splanchnicus* (Figure 3F). In *S. mansoni*-infected individuals with liver fibrosis, species such as *Rothia mucilaginosa, Turicibacter sanguinis, Veillonella atypica, Veillonella infantium, Lactococcus petaurid,* and *Holdemanella biformis* were enriched, whereas *Roseburia hominis* and *Clostridium disporicum* were depleted (Figure 3G). These findings indicate that distinct abundances of 17 candidate gut microbial species are associated with *S. mansoni* infection and the resulting liver fibrosis, demonstrating a consistent pattern across genetically diverse individuals.

Two gut bacterial species as reliable biomarkers of *S. mansoni* infection and associated liver fibrosis in Humans

We next evaluated the accuracy and stability of the 17 candidate microbial biomarkers associated with *S. mansoni* infection and liver fibrosis (Figures 3F & 3G) by quantified the abundance of these microbial candidate by targeted qPCR-based quantification in stool DNA samples from an independent validation cohort of age- and gender-matched SAC (KK+US+, n = 7; KK+US-, n=9; KK-US-, n=11; Table S2 and Supplementary Material 2).

Table S2: **Characteristics of the selected participants for the validation phase by species-specific real-time quantitative PCR.**

Factors	KK+US+ (n=7)	KK+US- (n=9)	KK-US- (n=11)	p-values
Age (years) range :	[9-11]	[8-15]	[9-15]	0.04
Mean (SD)	10 (1.00)	11.44 (2.24)	12.45 (1.91)	
Sex ratio (Male/Female)	1/6	5/4	5/6	0.97
BMI	15.75	16.45	17.11	0.17
Mean (SD)	(0.97)	(1.83)	(1.63)	
Length of residence (years) Mean (SD)	2 (NA)	8 (NA)	8 (2.82)	0.83
Freq Contact with water/day: Mean (SD)	1.00 (1.00)	1.66 (1.32)	1.27 (1.48)	0.57
Eggs Burden	447.4	84.00	0	0.08
Median (range)	(12-2496)	(12-588)	(0)	
PPF grades				
Possible PPF	06	00	00	NA
PPF	01	00	00	NA
Advanced PPF	00	00	00	NA

KK(+): Kato katz positive (*S. mansoni* eggs-positive); KK(-): Kato katz negative (*S. mansoni* eggs-negative); US(+): Positive for ultrasonography (clearly defined hepatic fibrosis); US(-): Negative for ultrasonography (No hepatic fibrosis); BMI: Body Mass Index; PPF: Periportal fibrosis; SD: standard deviation; Freq: Frequency; n: number; PPF: Periportal fibrosis; NA: Not applicable.

Species-specific primers (Table S3) were designed and optimized for single-band amplification with efficiencies of 87-105% and normalized to 16srRNA as a bacterial

552 housekeeping gene to relatively quantify bacterial abundance in normalized amounts of
553 stool DNA between participants and groups (as reported [27]).

554

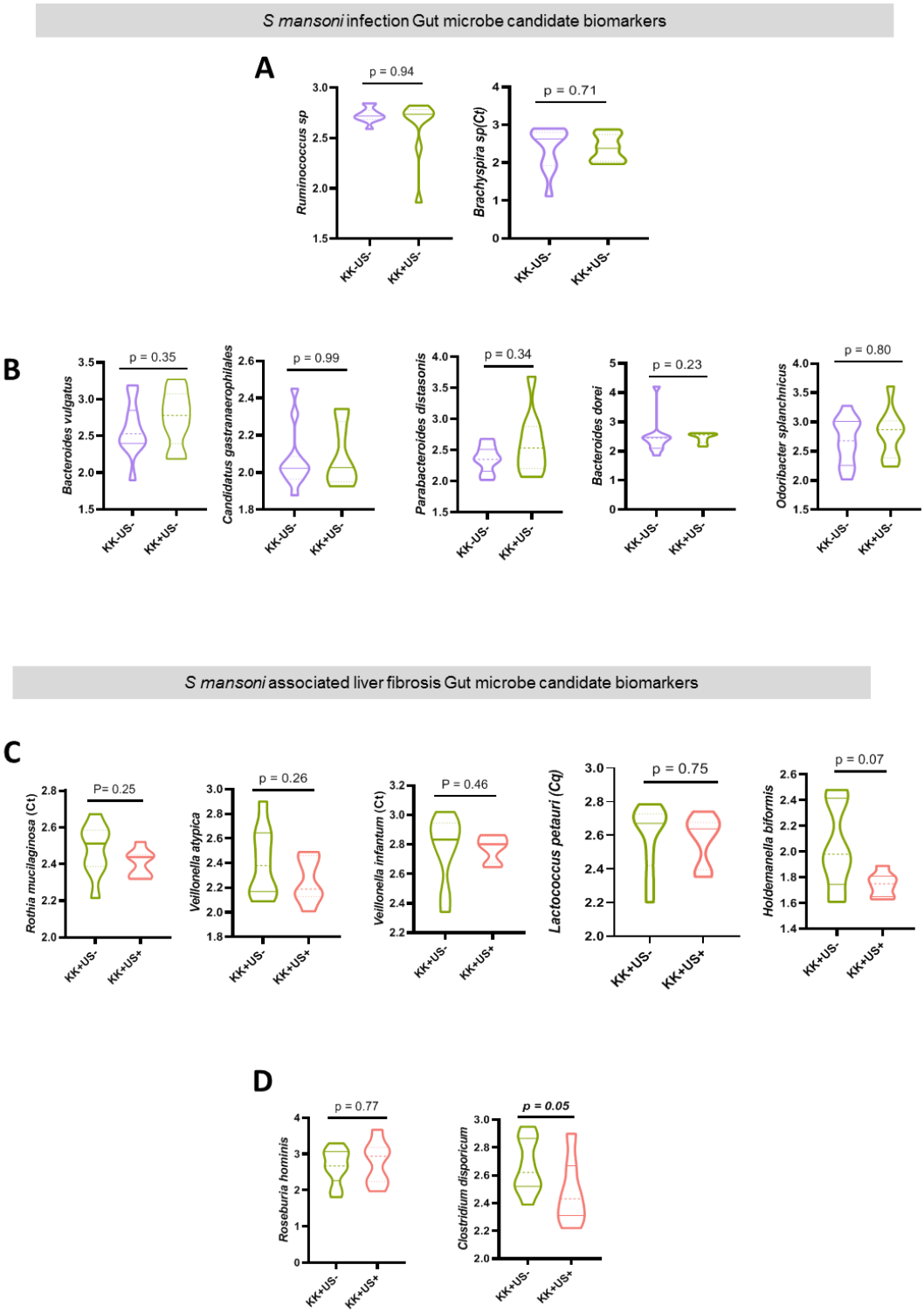
555 **Table S3**: **Microbial species-specific primers used for qPCR-based quantification of the candidate**
556 **microbes in stool DNA samples for validation.** Amplification optimal annealing temperature and qPCR
557 efficiency values are provided.

N°	Microbial species	Primers	Annealing Temperature	qPCR Effiency (%)
1	*Roseburia hominis*	GyA118F : CGTATTACCTCCGGTGTCAAG	53	104,10
		GyA118R : CGGTCAGAAGCTCAGAAGTATC		
2	*Clostridium disporicum*	Cpn130F : GCTGGTGCAAACCCAATGTT	51	100,06
		Cpn130R : ACCTATTTCATCATCAGCTGCTGA		
3	*Rothia mucilaginosa*	Cpn143F : GAAGTTGAGACCGAGGAAGAG	54	99,77
		Cpn143R : AGACCGAAAGTGTTGGAGTC		
4	*Turicibacter sanguinis*	Gro143F : GCAGGTGCAAATCCAATGAC	53	104,78
		Gro143R : TCCTCATCAGCTGCAGAAATAG		
5	*Veillonella atypica*	Rpo119F : CATGGAATATTTCGGCACTGAAG	51	101,67
		Rpo119R : TAGCACGAGCTTCTTCGATATG		
6	*Veillonella infantium*	Rpo93F : TTCCGATGGTACTCCGTACA	51	87,12
		Rpo93R : CCCAACCCAAGTGAGTTTCA		
7	*Lactococcus petauri*	Rpo128F : GCACCGATTCATGTGACTTTC	54	93,75
		Rpo128R : CGTTCAGAACCGTTGTTGATG		
8	*Holdemanella biformis,*	sRNA138F: TCAGACTGCCGGTGATAAAC	53	107,71
		sRNA138R : CTTTATGAGATTCGCTTGCCTTC		
9	*Bacteroides vulgatus,*	GyrA99F : AAAGCACCGGATTTCCCTAC	53	102,91
		GyrA99R : CTTAGCACGCATCACTACTCTAC		
10	*Parabacteriodes distasonis*	GyrA97F : GTCATTGTTTCACGTGCTCTTC	53	105,35
		GyrA97R : CGGATGTGTTACCCAGTTCAT		
11	*Bacteroides ovatus*	GyrA101F : GACCAGATTGGTTCGGTATGT	52	104,78
		GyrA101R : TCAGCATTCGGATCACTCAC		
12	*Bacteroides dorei*	recA111F : AGAAGTAATCGGCAACCAGAC	53	104,82
		recA111R : CCAGCTCTTGAGATACCTTCAC		
13	*Odoribacter splanchnicus,*	recA133F : GAGACAGTGTCATGGGCTTAC	53	101,33
		recA133R : CCGAACATCACTCCGATCTTATC		
14	*Ruminococcus sp CAG 330*	Rum120F : TGCCCTTCATGGTTTTAGGC	54	102,65
		Rum120R : ACAAGGGTGTATTGCATCGC		
15	*Brachyspira sp CAG 700*	sRNA121F : GAGATATGTCAGACCGCAAGG	54	100,92
		sRNA121R : TCGGTAGCAACAAAGGGTAAG		
16	*Candidatus Gastranaerophilales bacterium HUM 9*	Wg132F : ACCACGACCTGTTTCGTAAG	54	100,92
		Wg132R : ATCGCCCTAATCGACAATCC		
17	Housekeeping gene (Clifford et al., 2012)	sRNA180F: TCCTACGGGAGGCAGCAGT	51, 52, 53,54	103,09
		sRNA180R : TATTACCGCGGCTGCTGGC		

558

559

Species-specific qPCR quantification was consistent with metagenomic sequencing for two gut microbial species, which emerged as robust biomarkers of gut microbiome alterations during schistosomiasis (Figure 4). *B. ovatus* maintained its infection-associated profile, showing a significant reduction in infected SAC compared to uninfected controls (P = 0.01; Figures 4A & 4B). Conversely, *T. sanguinis* exhibited a fibrosis-associated profile, with significantly increased abundance in infected SAC with liver fibrosis compared to those without liver fibrosis (P = 0.02) (Figures 4C & 4D, and Supplementary Material 3). Species-specific qPCR-based quantification did not confirm significant abundance changes for 15 of the candidate microbes initially identified by metagenomics sequencing at the discovery phase (Figure S2). Although some bacterial taxa showed trends consistent with the discovery shotgun metagenomics dataset, these did not reach statistical significance, likely reflecting reduced effect sizes in the validation cohort.



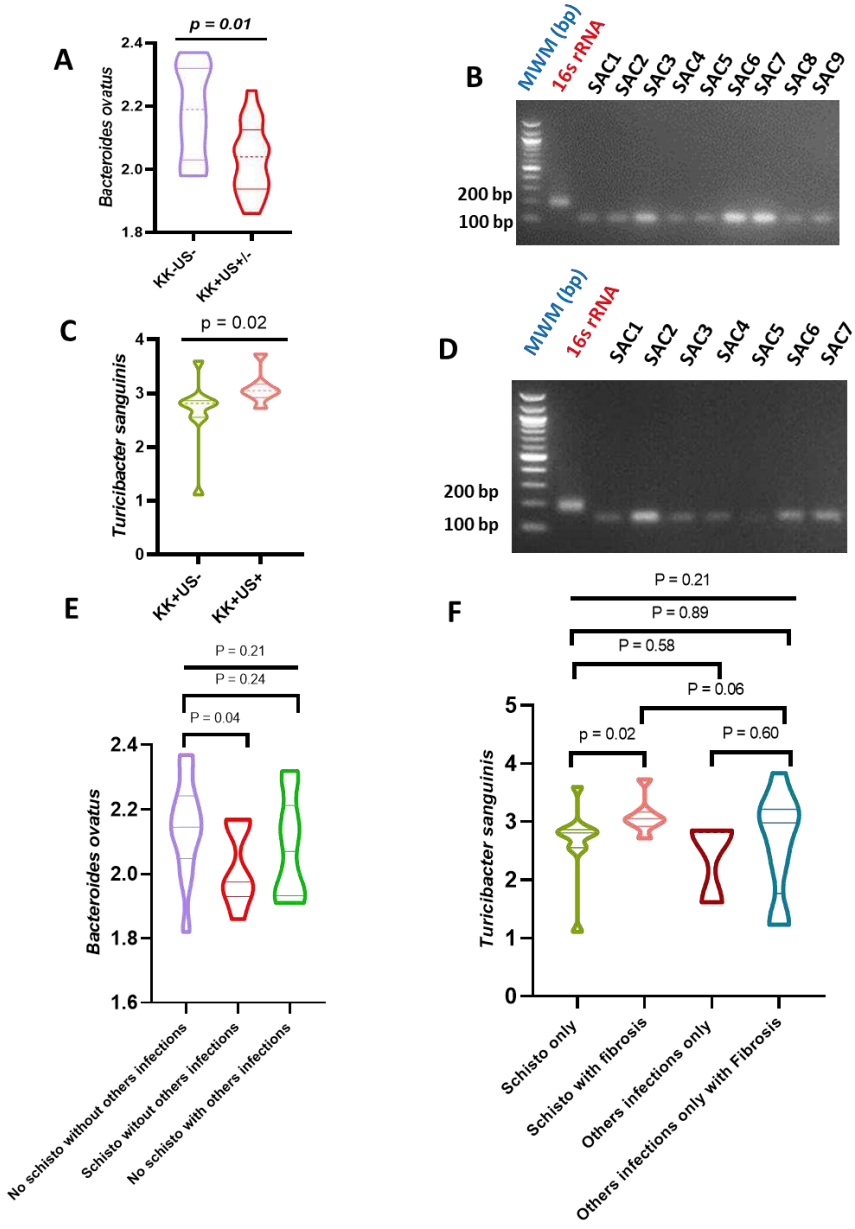
574

575 **Figure S2**: **qPCR-based validation of candidate biomarking gut microbes on a second cohort of**
576 **SAC.** Upper panels represent the relative abundance of the microbes previously identified by
577 metagenomics sequencing as differentially represented between healthy (KK-US-) and infected SAC

(KK+US-) without liver fibrosis i.e. **A.** pro-infection candidate biomarkers: (*Ruminococcus sp CAG 330*; *Brachyspira sp CAG 700*); **B.** Anti-infection candidate biomarkers: (*Bacteroides vulgatus; Candidatus gastranaerophilales Bacterium HUM9; Parabacteroides distasonis; Bacteroides dorei; Odoribacter splanchnicus*). Lower panels represent the relative abundance of the microbes previously identified by metagenomic sequencing as differentially represented between *S. mansoni*-infected (KK+US-) and infected with liver fibrosis SAC (KK+US+) **C**. Pro-fibrosis candidate biomarkers: (*Rothia mucilaginosa; Veillonella atypica; Veillonella infantum; Lactococcus petauri; Holdemanella biformis*); **D.** Anti-fibrosis candidate biomarkers: (*Roseburia hominis; Clostridium disporicum*). Validation qPCR were done with species-specific primers on a second subset of stool DNA from SAC termed validation cohort.

To exclude confounding effects of concomitant infections [28] we assessed *B. ovatus* and *T. sanguinis* relative abundance of in stool DNA from SAC with malaria, hepatitis, or soil-transmitted helminthiases (Figures 4E & 4F). Neither condition significantly altered *B. ovatus* levels (P = 0.24; Figure 4E) as observed with *S. mansoni* infection. Likewise, enrichment of *T. sanguinis* was observed only in *S. mansoni*-associated liver fibrosis, but not in fibrosis linked to other infections. Taken together, these results suggested that the two identified gut microbial changes are specific to *S. mansoni* infection (*B. ovatus*) and *S. mansoni*-associated associated liver fibrosis (*T. sanguinis*).

Using the qPCR quantification data from validation cohort, we generated the Receiver Operating Characteristic curve to assess the predictive accuracy of *B. ovatus* and *T. sanguinis*. Both biomarkers showed strong performance, with AUC values of 0.78 for *B. ovatus* (Figure 4G) and 0.82 for *T. sanguinis* (Figure 4H). These findings highlight their clinical potential as robust biomarkers of schistosomiasis infection and associated morbidity in SAC.

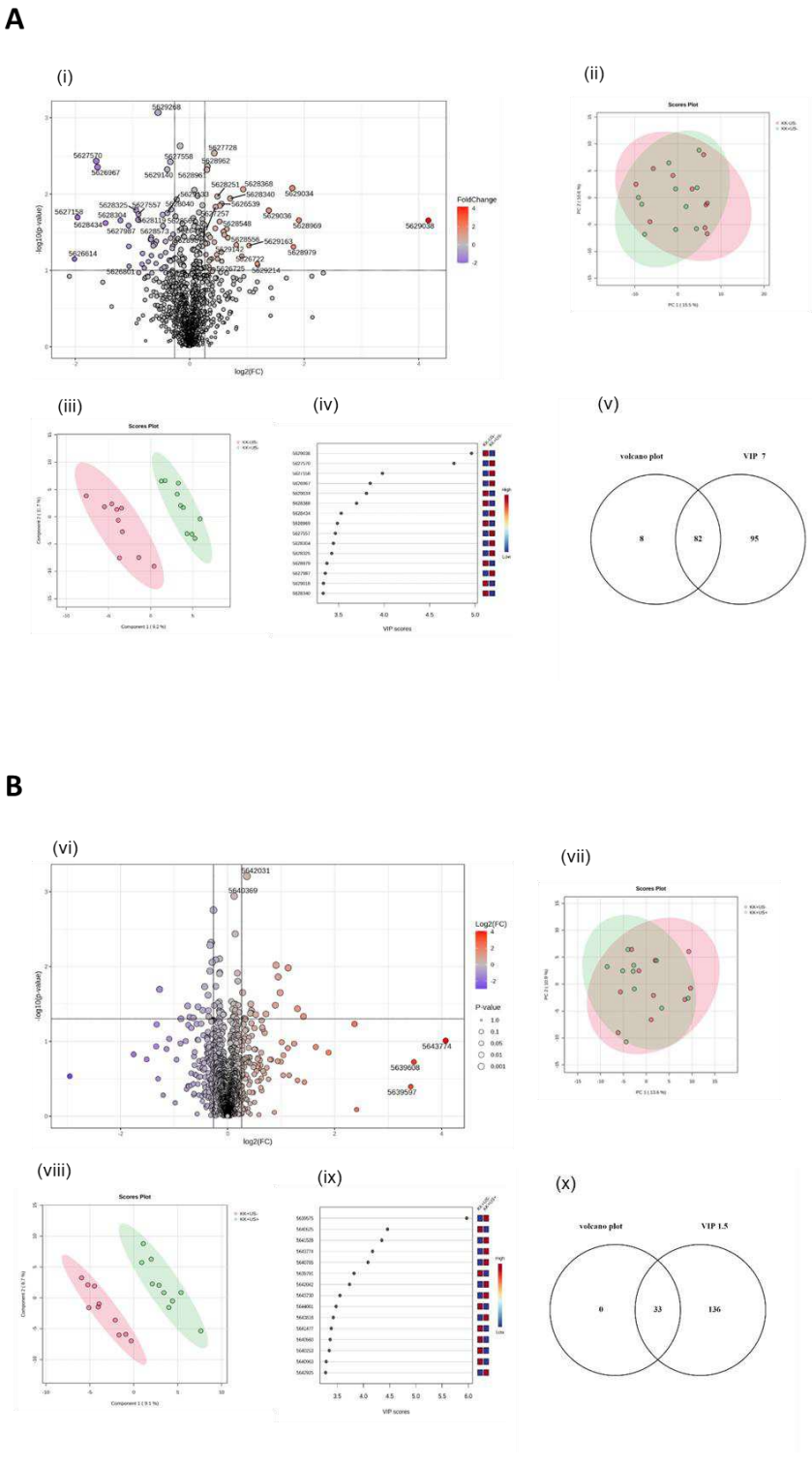

A
p = 0.01
Bacteroides ovatus
KK-US-
KK+US+/-
B
MWM (bp)
16s rRNA
SAC1
SAC2
SAC3
SAC4
SAC5
SAC6
SAC7
SAC8
SAC9
200 bp
100 bp
C
p = 0.02
Turicibacter sanguinis
KK+US-
KK+US+
D
MWM (bp)
16s rRNA
SAC1
SAC2
SAC3
SAC4
SAC5
SAC6
SAC7
200 bp
100 bp
E
P = 0.21
P = 0.24
P = 0.04
Bacteroides ovatus
No schisto without others infections
Schisto witout others infections
No schisto with others infections
F
P = 0.21
P = 0.89
P = 0.58
P = 0.06
p = 0.02
P = 0.60
Turicibacter sanguinis
Schisto only
Schisto with fibrosis
Others infections only
Others infections only with Fibrosis
G
ROC of B. ovatus in S. mansoni infection
Sensitivity%
AUC = 0.78
CI = 0.60 - 0.96
100% - Specificity%
H
ROC of T. sanguinis in fibrosis during S. mansoni infection
Sensitivity%
AUC = 0.82
CI = 0.60 - 1.00
100% - Specificity%

602

Figure 4: Validation of *Bacteroides ovatus* and *Turicibacter sanguinis* as biomarkers of *S. mansoni* infection and/or liver pathology by qPCR on a secondary SAC cohort. Relative abundance of *B. ovatus* (**A**) and gel electrophoresis confirmation of single band product after qPCR (**B**) amplification of the target *B. ovatus* specific gene and housekeeping bacterial 16s rRNA gene. Relative abundance of *T. sanguinis* (**C)** and gel electrophoresis confirmation of single band product after qPCR (**D**) amplification of the target *T. sanguinis* specific gene and housekeeping bacterial 16s rRNA gene. **(E**) Assessment of disease specificity of gut levels of *B. ovatus* as biomarker of *S. mansoni* infection in settings of other infections with malaria, hepatitis and/or STH. (**F**) Assessment of disease specificity of gut levels of *T. sanguinis* as biomarker of *S. mansoni* infection-associated liver fibrosis in settings of liver fibrosis associated with other diseases i.e. malaria, hepatitis and/or STH infections. (**G**) Diagnostic performance of gut microbial levels of *B. ovatus* for *S. mansoni* infection in SAC. (**H**) Diagnostic performance of gut microbial levels of *T. sanguinis* for *S. manson*i-associated liver fibrosis among *S. mansoni* infected SAC. ROC: Receiver Operating Characteristic; AUC: Area Under the Curve; CI: Confidence Interval; SAC: School-aged Children; MWM: Molecular Weight Marker; Bp: base pairs; ns= non-significant i.e. $p<0.05$

Comparable metabolomic profiles of *S. mansoni*-infected children and identified gut signature microbes

To investigate gut microbiome regulation of schistosomiasis, we analysed the microbial metabolome of identified reliable biomarkers in relation to host plasma metabolites. Untargeted LC/MS metabolomics of SAC from the discovery cohort revealed distinct metabolic signatures associated with *S. mansoni* infection and associated liver fibrosis (Figure S3, and Supplementary Material 4 and 5). In the infection model (KK+US- vs KK-US-), integration of volcano plot and VIP selections identified 82 high-confidence biomarkers meeting both statistical and multivariate discrimination criteria (Figure S3A-v). In the fibrosis model (KK+US+ vs KK+US-), volcano plot and VIP integration identified 33 high-confidence biomarkers (Figures S23-vii, viii). These high-confidence biomarkers represent priority candidates for further investigation through network-based metabolic source attribution.



631

632 **Figure S3. Plasma metabolite changes during schistosomiasis: (A) Infection model (KK+US- vs KK-**
633 **US-).** (i) Volcano plot of plasma metabolite profiles comparing infected without liver fibrosis versus unifected
634 SAC. (ii) PCA - PERMANOVA showed no significant differences (*P* = 0.588) between infected without liver

fibrosis (KK+US-) and healthy control group (KK-US-). **(iii)** PLS-DA distinguished infected SAC without liver fibrosis from controls. **(iv)** VIP analysis highlighted 15 key metabolites (VIP scores >1.5) **(v)** Venn diagram showed overlap between volcano and VIP-selected features (185 metabolites). **(B) Fibrosis model (KK+US+ vs KK+US-)**. (vi) Volcano plot of plasma metabolite profiles comparing SAC infected with liver fibrosis (KK+US+) versus infected without liver fibrosis (KK+US-). (vii) PCA - PERMANOVA showed no significant differences (P = 0.433) in plasma metabolite changes between the two groups (viii) PLS-DA distinguished fibrosis cases from non-fibrosis infections. (ix) VIP analysis highlighted 15 key metabolites (VIP scores >1.5). (x) Venn diagram showed overlap between volcano and VIP-selected features (169 metabolites). The intensity of the colored boxes on the right represents the relative abundance of the corresponding metabolite in each group.

Reasoning that the identified high-confidence biomarkers could be produced by the human host, commensal microbes or the both, we extended our framework to plasma metabolites, partitioned by predicted origin using AMON analysis tool to refine organism-specific metabolic interplay[24] (Figure S4). In the *S. mansoni* infection model, 82 metabolic peaks yielded 1,961 metabolic features (Figure S4A), of which 250 were uniquely attributable to *B. ovatus* (gene set 1), 1,166 to the human host (gene set 2), and 499 shared between human host and *B. ovatus*. In *S. mansoni*-associated liver fibrosis,33 peaks corresponded to 1,867 metabolic features (Figure S4B), including 184 exclusives to *T. sanguinis*, 1,274 human host-derived, and 391 shared. An additional 18 metabolic features fell outside the predicted origin, suggesting alternative sources such as diet, environment, or uncharacterized microbial activity. To investigate the metabolic interplay between gut microbes and the host during *S. mansoni* infection and its associated liver fibrosis, we performed KEGG-based pathways analysis on metabolites predicted to originate exclusively from *B. ovatus* and *T. sanguinis* as well as those attributed solely to host in each context (Figure S4, [24, 29]).

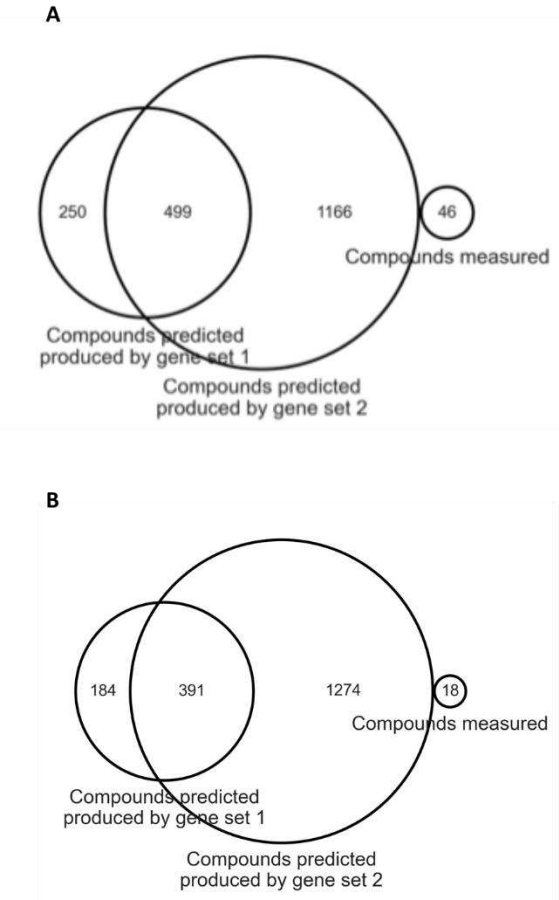
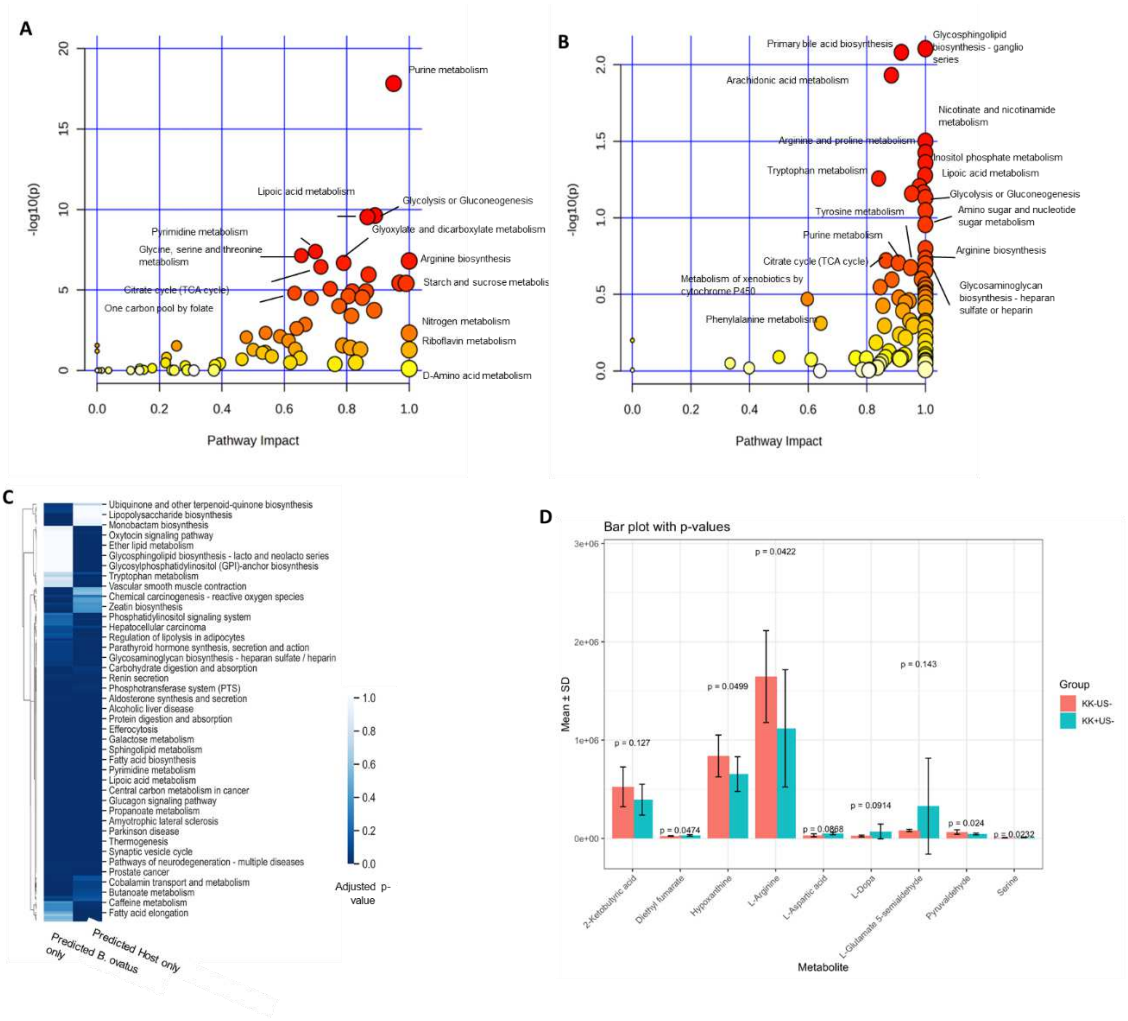


Figure S4. **Venn Diagram illustrating overlaps in compound sets following AMON analysis. (A)** The Venn diagram displays overlaps among compound sets potentially generated by *Bacteroides ovatus* (gene set 1), Homo sapiens (gene set 2), both, and the measured metabolites in KK+US- and KK-US- plasma groups. Totally, 1961 compounds were measured form plasma metabolomics analysis. Predicted partitions include: 250 compounds uniquely attributable to *B. ovatus*, 1,166 to the host, 499 to both organisms (indicative of shared metabolic pathways), and 46 compounds uniquely present among measured metabolites but not predicted by either gene set, pointing to alternative origins. **(B)** The Venn diagram depicts overlaps among compound sets potentially attributable to *Turicibacter sanguinis* (gene set 1), *Homo sapiens* (gene set 2), both, and the total pool of metabolites actually measured in the plasma by untargeted LC/MS with KEGG annotation (distinguishing KK+US+ from KK+US- samples). The analysis focuses on compounds present in the measured metabolite list submitted, integrating gene set predictions to enable pathway analysis. The segment labeled “Compounds measured” represents the full set of detected plasma metabolites (n = 1,867), comprising those solely produced by gene set 1 (184), those overlapping with gene set 1 and gene set 2 (391), those specific to gene set 2 (1,274), and those unique to the measured set but not predicted by either gene set (18), the latter possibly indicating environmental, dietary, or unknown microbial sources.

In the infection model, *B. ovatus* contributed 250 exclusive metabolic features with broad enrichment across core metabolic pathways (Figure 5A). The most enriched pathway was purine metabolism, which remained dominant (52/70 matched, $p = 1.18 \times 10^{-}18$, impact = 0.95). Additional highly enriched pathways included glycolysis/gluconeogenesis (p = 2.38×10^{-10}, impact = 0.89), and lipoic acid metabolism ($p = 2.91 \times 10^{-10}$, impact = 0.87). Other pathways of significant enrichment encompassed arginine biosynthesis ($p = 1.58 \times 10^{-7}$, impact = 1.0), glyoxylate and dicarboxylate metabolism ($p = 2.12 \times 10^{-7}$, impact = 0.79), and the tricarboxylic acid (TCA) cycle ($p = 3.70 \times 10^{-7}$, impact = 0.72).



687

688 **Figure 5: Comparative microbiome/host-specific metabolic pathway analyses.** (A) *B. ovatus* pathway
689 analysis, (B) Host-Exclusive Metabolic Pathways During Asymptomatic *S. mansoni* Infection (*Infection*
690 Model), (A, B) The size and colour intensity of dots represent the magnitude of enrichment and statistical
691 significance, respectively. (C) Heatmaps showing the *p*-values associated with both corresponding pathway
692 enrichment analyses with KEGG pathways. The first column is respectively p-values for enrichment of
693 KEGG pathways in compounds that were detected via untargeted LC/MS of plasma and predicted
694 generated by members of the fecal microbiome *(Bacteriodes ovatus) (left column) and the human host*
695 *(right column).* (D) Individual metabolites analysis.

696

697

Carbohydrate-related pathways such as starch and sucrose metabolism ($p = 3.90 \times 10^{-6}$, impact = 0.99) and fructose and mannose metabolism ($p = 3.73 \times 10^{-6}$, impact = 0.97) were also significantly enriched (Table S4 and Supplementary Material 6). Individual metabolites analysis from *B. ovatus* (Figure 5D) revealed significant decreases in hypoxanthine (p = 0.049), L-arginine (p = 0.042) and pyruvaldehyde (p = 0.024), alongside an increase in L-Dopa (p = 0.09).

Table S4. *B. ovatus* pathway analysis showing the top 10 enriched pathways

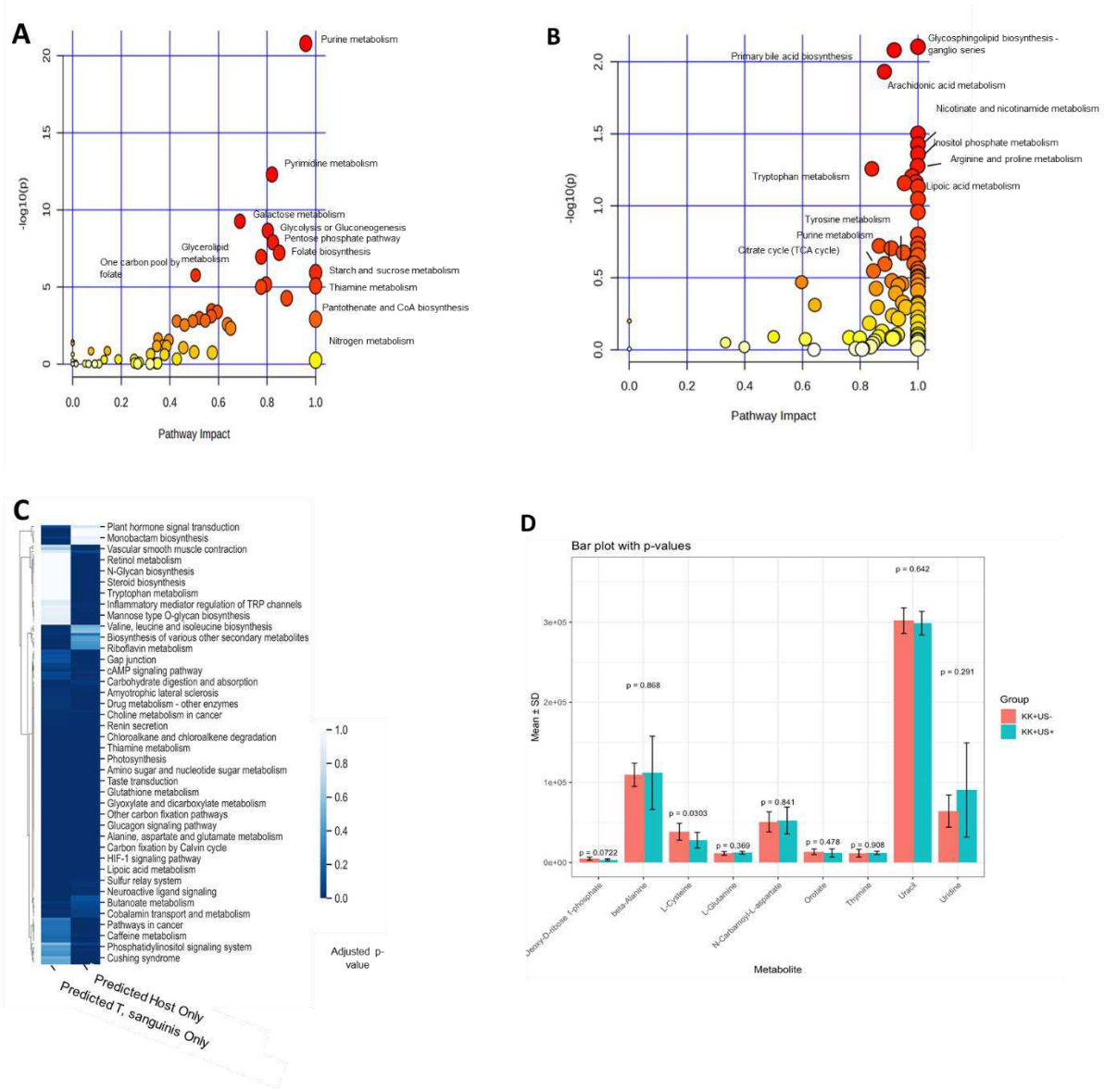
Pathway Name	Match Status	p	-log(p)	FDR	Impact
Purine metabolism	52/70	1.48E-18	17.83	1.18E-16	0.95011
Glycolysis or Gluconeogenesis	22/26	2.38E-10	9.6234	7.76E-09	0.89048
Lipoic acid metabolism	23/28	2.91E-10	9.5361	7.76E-09	0.86629
Pyrimidine metabolism	26/39	4.10E-08	7.3867	8.21E-07	0.69969
Glycine, serine and threonine metabolism	23/33	7.34E-08	7.1341	1.18E-06	0.65446
Arginine biosynthesis	13/14	1.58E-07	6.8008	2.11E-06	1
Glyoxylate and dicarboxylate metabolism	22/32	2.12E-07	6.6745	2.42E-06	0.79001
Citrate cycle (TCA cycle)	16/20	3.70E-07	6.4315	3.70E-06	0.71705
Pentose phosphate pathway	17/23	1.12E-06	5.9521	9.93E-06	0.86978
Fructose and mannose metabolism	15/20	3.73E-06	5.4283	2.84E-05	0.96964
Starch and sucrose metabolism	14/18	3.90E-06	5.4091	2.84E-05	0.99026
Pyruvate metabolism	16/23	8.56E-06	5.0677	5.70E-05	0.74706
Alanine, aspartate and glutamate metabolism	18/28	1.24E-05	4.9063	7.11E-05	0.81731

KEGG-based pathways analysis of the184 metabolic features attributed exclusively to *T. sanguinis* revealed significant enrichment of nucleotide metabolism (Figure 6). Purine metabolism emerged as the top enriched pathway, with 49 of 70 matched, a highly significant P =1.6137E-21 and the highest impact score (0.96). Pyrimidine metabolism was also strongly enriched (28/29 matches, P = 5.0636E-13, impact = 0.82). Carbohydrate-related pathways showed marked enrichment. Galactose metabolism (20/27 matches, P = 5.4967E-10, impact = 0.68) and glycolysis/gluconeogenesis (19/26 matches, P = 2.2544E-09, impact = 0.80) were significantly impacted. Starch and sucrose

714 metabolism also reached significance (*P* = 1.1715E-06) with the highest possible impact
715 score (1.0).

716 Folate-associated pathways were consistently enriched. Both folate biosynthesis (18/27
717 matches, *P* = 6.0897E-08, impact = 0.85) and the one-carbon pool by folate (16/26
718 matches, *P* = 1.7348E-06) were significantly perturbed. Lipid metabolism was also
719 affected, with glycerolipid metabolism (13/16 matches, *P* = 1.1121E-07) showing strong
720 enrichment.

721



722

723 **Figure 6. Comparative microbiome/host-specific metabolic pathway analyses: (A)** *T. sanguinis*
724 pathways analysis, **(B)** Host-exclusive metabolic pathways during *S. mansoni*-associated liver fibrosis
725 (*Liver fibrosis* Model). **(A, B)** The size and color intensity of dots represent the magnitude of enrichment
726 and statistical significance, respectively. **(C)** Heatmaps showing the *p*-values associated with both
727 corresponding pathway enrichment analyses with KEGG pathways. The first column is respectively p-
728 values for enrichment of KEGG pathways in compounds that were detected via untargeted LC/MS of
729 plasma and predicted generated by members of the fecal microbiome *(T. sanguinis)* (left column) and the
730 human host (right column).

731

Finally, amino acid metabolism was represented by alanine, aspartate, and glutamate metabolism (16/28 matches, *P* = 6.8279E-06) (Table S5 and Supplementary Material 7).

Table S5. *T: sanguinis* pathway analysis showing the top 10 enriched pathways

Pathway Name	Match Status	p	-log(p)	FDR	Impact
Purine metabolism	49/70	1.6137E-21	20.792	1.2909E-19	0.95946
Pyrimidine metabolism	28/39	5.0636E-13	12.296	2.0254E-11	0.82017
Galactose metabolism	20/27	5.4967E-10	9.2599	1.4658E-08	0.68828
Glycolysis or Gluconeogenesis	19/26	2.2544E-09	8.647	4.5088E-08	0.8031
Pentose phosphate pathway	17/23	1.2708E-08	7.8959	2.0334E-07	0.82405
Folate biosynthesis	18/27	6.0897E-08	7.2154	8.1196E-07	0.84979
Glycerolipid metabolism	13/16	1.1121E-07	6.9538	1.271E-06	0.77569
Starch and sucrose metabolism	13/18	1.1715E-06	5.9312	1.1715E-05	1.0
One carbon pool by folate	16/26	1.7348E-06	5.7608	1.542E-05	0.50588
Alanine, aspartate and glutamate metabolism	16/28	6.8279E-06	5.1657	5.4623E-05	0.79568

Collectively, these findings demonstrate that Exclusive metabolic features from *B. ovatus* and *T. sanguinis* span nucleotide, carbohydrate, folate, lipid, and amino acid pathways, highlighting complementary microbial roles in reshaping host metabolism during *S. mansoni* infection and associated liver pathology.

DISCUSSION

Schistosomiasis remains a major cause of morbidity, with increasing evidence indicating that its regulation may be influenced by the gut microbiome.[15, 30]. The gut microbiome

746 is composed of a complex and dynamic community of microorganisms that significantly
747 impacts the host's health both during homeostasis and disease such as
748 schistosomiasis[31]. However, the depth of schistosomiasis regulation by the gut
749 microbiome is still poorly and inconclusively known. The comprehensive assessment of
750 all reports, making use of fragmented and mutually exclusive pieces of either
751 experimental animal studies [30] or field surveys on humans [15, 30], only agreed, until
752 date, to the fact that schistosomiasis presents with a significant alteration of the structure
753 and composition of the host gut microbiome leading to dysbiosis[15].

754 To build on this foundational knowledge, we explored the interrelationship between the
755 commensal microbiota, the host, and the parasitic helminth *S. mansoni* during chronic
756 schistosomiasis through animal and human investigations. First, we demonstrated that a
757 transferable gut microbiota plays a causal role in regulating the pathogenesis of *S.*
758 *mansoni* in mouse breeds with varying susceptibility to chronic schistosomiasis. We then
759 found that SAC, despite genetic differences, exhibit gut microbial profiles that are
760 characteristic of either *S. mansoni* infection or the development of liver fibrosis following
761 the infection.

762 The combination of animal model with human data, effectively addressing several
763 challenges faced by previous research on schistosome-microbiome interactions. [15, 30]
764 [30]. Past studies were confounded by the fact that in the laboratory, animal models,
765 although mechanistically flexible, cannot offer a direct reflection of the human gut
766 microbiome dynamics [16]; and in the field, most human studies do usually rely on non-
767 validated high-throughput sequencing-based investigations on highly variable and
768 superficially phenotyped individuals (age, gender, BMI etc.) [30, 32] that are too unstable

to ensure careful inferences and reproducibility. Our approach combines the use of well-controlled mouse breeds with carefully phenotyped age- gender-matched carefully phenotyped human cohorts (repeated stool microscope-based examinations for *S. mansoni* infection status and abdomen ultrasonography for liver pathology), which mitigates of most of the above limitations, enabling a robust appraisal of the gut microbiome's role during schistosomiasis. Building on this methodological strategy, we have taken existing knowledge a step further by testing 3 postulates to unequivocally address the role of the host gut microbiome during schistosomiasis.

Postulate 1: Gut microbiome plays a causal role in regulating schistosomiasis pathophysiology, as inspired by literature [33]. We made use of the known coprophagic nature of mice [34] to test how FMT, through co-housing [25, 35] of genetically different breeds of mice with differential susceptibility to schistosomiasis, would affect the course of experimental chronic schistosomiasis. Our findings show that susceptible SPF2 C57BL/6 mice became more resistant to *S. mansoni* infection, after co-housing with resistant SPF1 C57BL/6 mice, confirming the gut microbiome's causal role in reducing schistosomiasis morbidity. Notably, resistant SPF1 C57BL/6 mice did not become more susceptible, indicating that resistance is mediated by transferable gut microbes, while susceptibility arises from their absence. This unidirectional pheno-conversion strongly argues for resistance to schistosomiasis as being mediated by the presence of (a) specific gut microbe(s) that can be transferred to a recipient host whereas susceptibility, that does not appear to be transferable, to occur as a result of the absence of this(ese) protective microbe(s). These results support the development of microbiome-

based therapeutics [30] for schistosomiasis and highlight the importance of interpreting discrepancies in experimental studies, where genetic identicality may not guarantee consistent susceptibility due to varying husbandry conditions [36, 37]. Establishing a gut microbiome normalization framework is essential for comparability across studies. Future research involving diverse mouse breeds with humanized microbiomes or large human datasets could identify microbes that control schistosomiasis morbidity. Such studies should assess gut microbial changes and correlated them with specific microbial profiles, [38, 39]. While environmental factors could explain the increased resistance observed, the controlled husbandry conditions (BSL2 units for small animal experimentation whereby diet, husbandry, light cycles, temperature are all similar for hosted animals kept under individually ventilated cages at the same animal density i.e. 8/cage in our settings) strongly suggest that fecal microbiota transfer (FMT) from coprophagy drives the changes in disease course. Follow-up studied on gut microbial profile changes before and after co-housing would certainly help identify specific microbes responsible for resistance transfer.

The differential genetic backgrounds of the tested mouse breeds indicate that FMT can override genetic susceptibility, aligning with findings in other conditions such as type 1 diabetes [40-42], autism spectrum disorder[43-45], which further support microbiome-based therapeutics against schistosomiasis.

The associated pathognomonic feature of microbiome regulation was peri-ova granulomatous inflammation, consistent with previous reports that the gut microbiome depletion by antibiotics and anti-mycotics reduced intestinal granuloma development[11]. In fact, the exacerbated liver peri-ova granulomatous inflammation observed in susceptible animals, which improve after co-housing with resistant mice, suggests an

immunomodulatory role of the transferable gut microbe(s) on the granulomatous response(s). This is consistent with the established fact that hosts that immunoregulate schistosomiasis-induced inflammatory responses cope better with the disease [4-7]. Identifying these microbes and their produced metabolites and immune pathways will enhance our understanding of microbiome-based strategies against schistosomiasis.

To translate these findings into clinical applications, validating results in outbred mice or humanized mice is crucial, as they better resemble human genetic and microbiota diversity more closely mimicking the elevated diversity in the human population [46] than inbred mice. Additionally, using human samples with similar disease phenotype alterations will provide a robust platform for exploring commensals linked to host resistance against infection and pathology. This warranted our next series of investigations in this study and the second postulate.

Postulate 2: Specific gut microbe(s) associate significantly and robustly with schistosomiasis in humans. To address, through this postulate, our quest to uncover the role of the gut microbiome during human schistosomiasis, we analyzed gut microbial communities in school-aged children from an endemic area. Study participants were strictly phenotyped and clustered by *S. mansoni* infection, co-occurring diseases (malaria, hepatitis, STH), and liver fibrosis grade. Age- gender-matching of the clustered individuals uniquely enabled here the circumvention of hitherto overlooked confounding factors. Altogether, these measures also resulted in a relative cultural compactness of the enrolled participants to ensure comparable feeding habits[47]. Screening involved shotgun metagenomics sequencing of a subset of participants' DNA samples (discovery

cohort), further validated in a second subset (validation cohort) by qPCR and finally confirmed for specificity of candidate gut microbe profiles in participants harboring other concomitant infections (malaria, hepatitis, STH). This is an unprecedentedly stringent staircase approach that does ensure only the most robust and reliable biomarkers consistently appear as significantly different between the clustered participants' groups of interest.

Notably, our study revealed for the first time the depletion of *B. ovatus* in the gut of *S. mansoni*-infected SAC and an enrichment of *T. sanguinis* in the gut of *S. mansoni*-infected SAC that developed liver fibrosis. The uniqueness of our findings likely stems from the stringent enrolment, testing and validation processes compared to previous human studies[15, 30]. Our validation approach excludes biases from age/gender variability, erroneous significant differences from strictly sequencing-based studies and lack of specificity by inclusion of changes due to other infections likely to occur in the studied sites. By ruling out such caveats, gut microbial signature of schistosomiasis and its associated liver fibrosis in SAC is robust, though not necessarily exhaustive. In fact, as the present results are from a limited sampling through a cross-sectional study, it is difficult to completely rule out false negative cases. A larger longitudinal study with similar levels of selection, tracking changes in *S. mansoni* infection status and liver fibrosis grades change over time, would better address this limitation.

Our findings identify *B. ovatus* as a gut microbe biomarker negatively associated with *S. mansoni* (depletion in *S. mansoni*-infected SACs). Consistent with that is the fact that the gut health is usually compromised during *S. mansoni* infections [2, 48], and *B. ovatus* is known to have a beneficial role in maintaining a healthy gut ecosystem[49]. It helps digest

complex carbohydrates, produces short-chain fatty acids (SCFAs) like butyrate, interacts with the immune system while regulating the release of intestinal neurotransmitters[49] such as the elevation of the schistosomicidal neurotransmitter GABA[50]. The reduced abundance of such a gut protective bacterium, with schistosomicidal potential therefore stands to reason as a pathognomonic feature of *S. mansoni*-infected individuals. Yet, whether depletion of *B. ovatus* promotes susceptibility of S. mansoni or is actively suppressed by parasites remains unclear.

The exciting observation that another gut microbe, *T. sanguinis*, can reliably help differentiate *S. mansoni*-infected SAC from *S. mansoni*-infected SAC presenting with morbidity in the form of liver fibrosis is intriguing and unprecedented in its reach. In fact, *T. sanguinis* is responsible for several key processes but importantly lipid metabolism[51]. Of note, *T. sanguinis* fosters bile acid metabolism to release their unconjugated forms[51] which, when accumulating, can contribute to liver damage and fibrosis[52, 53]. This supports its role as a liver fibrosis biomarking bacterium during *S. mansoni* infection and provides ground to assess the needed steps for its longitudinal / causal validation. Such a confirmation could set the stage for the development thereafter of a novel non-invasive morbidity gut microbial biomarker to reliably monitor the onset/disappearance of liver fibrosis in *S. mansoni* cases and in so doing help the unequivocal appraisal of elimination of the disease as a public health problem. This bears the prospect of a unique programmatic value as a possible alternative to the sole use of the limited indicator that is the excreted egg burden to reliably monitor the level of schistosomiasis pathology in the field[8].

Postulate 3: Gut microbiome drives schistosomiasis via systemic metabolic shifts

B. ovatus-derived metabolites, including hypoxanthine, L-arginine, and pyruvaldehyde appear to be associated with *S. mansoni* infection. Hypoxanthine, is a substrate for efficient purine nucleotide biogenesis[54] and a source of energy for intestinal epithelial cells and enhance the ability of intestinal barrier recovery by decreasing oxygen consumption[55]. During S. *mansoni* infection, intestinal depletion of *B. ovatus* lead to significant drop of plasma hypoxanthine levels. This disrupts the energy supply for epithelial cell and weakens the intestinal barrier, driving the intestinal inflammation seen in active *S. mansoni* infection[56]. L-arginine, a semi-essential amino acid, plays a critical role in immune system through its involvement in polyamine metabolism, T-cell activity and the production nitric oxide (NO). NO has been associated with the defense against *Schistosoma*: in *S. mansoni,* it disrupts mitochondrial ultrastructure and aerobic energy metabolism[57], while in *S. japonicum*, it inhibits mitochondrial respiration, reducing worm survival and egg production[58]. During *S. mansoni* infection, intestinal depletion of *B. ovatus* and the resulting drop in plasma L-arginine compromise host immunity, increasing susceptibility and promoting parasite persistence. Pyruvaldehyde (methylglyoxal/2-oxopropanal) is a byproduct of cellular metabolism implicated in chronic diseases such as diabetes, neurodegenerative disorders (Alzheimer and Parkinson diseases), and cardiovascular diseases. In *S. mansoni*, elevated pyruvaldehyde impairs parasite viability by disrupting protein function, damaging DNA, and compromising essential processes like replication, protein synthesis and energy production. Consistent with intestinal *B. ovatus* depletion, plasma pyruvaldehyde levels drop significantly during *S. mansoni* infection.

907 Conversely, *T. sanguinis* displays a focused, high-impact metabolic profile, with
908 significantly enrichment in purine and pyrimidine metabolism. Consistently elevated
909 pathway impact scores highlight profound disruption of specific metabolic networks. Such
910 robust profiles likely drive metabolic competition and stress that exacerbates fibrotic
911 responses[59], whereas broader metabolic versatility with extensive host integration
912 supports complementation that maintains commensal homeostasis during parasitic
913 infection[60-62].

914 In *S mansoni* infection-associated liver fibrosis, reduced L-cysteine links *T. sanguinis*
915 activity to fibrotic progression via disrupted bile acid-taurine fuels bile acid conjugation in
916 hepatocytes[63]. However, *T. sanguinis* strains possess bile salt hydrolase activity that
917 deconjugates taurine-conjugated bile acids[51], liberating free taurine and unconjugated
918 bile acids in the intestinal lumen[64], and creating a futile cycle: hepatic L-cysteine is
919 repeatedly consumed for taurine resynthesis, depleting hepatic L-cysteine reserves. This
920 depletion cascades into disturbing liver fibrosis by bile acids homeostasis and
921 cysteine/glutathione metabolism through FXR-mediated suppression of cysteine
922 dioxygenase 1 (CDO1)[65, 66]. Indeed, schistosomiasis infection disrupts FXR signaling
923 and bile acid homeostasis, with FXR deficiency exacerbating liver damage in *S.*
924 *japonicum*-infected mice[67]. L-cysteine is the rate-limiting substrate for glutathione
925 (GSH) synthesis[68], and its depletion impairs antioxidant defenses against oxidative
926 stress in chronic schistosomiasis[69]. Glutathione deficiency further disrupts hepatic lipid
927 metabolism, lowering the expression of lipogenic regulators such as SREBP-1c and
928 triglyceride synthesis[70], contributing to the lipid metabolic alterations documented in
929 schistosomal liver fibrosis. The observed L-cysteine reduction in *S. mansoni* infection -

associated liver fibrosis emerges as a convergent metabolic signature linking *T. sanguinis* activity with bile acid modification, impaired antioxidant capacity, dysregulated lipid metabolism, and fibrogenic progression.

Significant enrichment of purine and pyrimidine metabolism in *T. sanguinis*-specific metabolites positions nucleotide metabolism as a central axis linking gut microbiome composition to liver fibrosis in schistosomiasis. Near-maximal pathway impact scores highlight profound disruption of nucleotide homeostasis with direct relevance to fibrogenesis. Hepatic stellate cell activation and transdifferentiation into myofibroblasts requires abundant nucleotide precursors for DNA synthesis, creating competition between bacterial replication and host tissue repair[59, 71, 72]. Likewise,, immune responses to *S. mansoni* infection-including granuloma formation and Th2 polarization - depend on lymphocyte clonal expansion, which may be impaired by bacterial consumption of nucleotide precursors[4, 59, 73-75]. Extracellular purines also act as signalling molecules via purinergic receptors (P2X, P2Y, adenosine receptors), with ATP driving pro-inflammatory responses and adenosine exerting context-dependent pro- or anti-fibrotic effects[76, 77]. Perturbation of this network by *T. sanguinis* may shift the ATP/adenosine balance toward pro-fibrotic signalling[78], consistent with elevated expression of Purine/pyrimidine in plasma metabolome and prior evidence linking nucleotide metabolism disturbances to fibrosis[79]. Furthermore, the L-cysteine–taurine–bile acid axis and nucleotide metabolism are interlinked: glutathione, synthesized from L-cysteine, protects DNA integrity during stellate cell proliferation. Thus, concurrent L-cysteine depletion and nucleotide metabolism perturbation by *T. sanguinis* represent

synergistic metabolic stress that amplifies fibrogenic progression in chronic schistosomiasis.

Analysis of host-specific metabolites revealed consistent enrichment in primary bile acid biosynthesis, glycosphingolipid biosynthesis, arachidonic acid metabolism, and cytochrome P450-mediated xenobiotic metabolism across both comparison schemes, validating AMON's accuracy in distinguishing eukaryotic metabolic capabilities. The enrichment of bile acid and arachidonic acid metabolism has direct mechanistic relevance to fibrosis, as disrupted bile acid homeostasis promotes hepatic stellate cell activation through FXR and TGR5 signaling[80, 81], while arachidonic acid-derived eicosanoids orchestrate inflammatory responses that can either promote or resolve fibrosis[80]. These findings have translational implications: targeting *T. sanguinis* through selective antimicrobials or promoting *B. ovatus* through prebiotics/probiotics could prevent fibrosis progression, while modulating nucleotide metabolism (adenosine receptor agonists/antagonists, inhibitors of bacterial purine biosynthesis) or one-carbon metabolism (folate supplementation to reduce metabolic competition) represents pathway-targeted therapeutic strategies. Critically, our findings suggest effective interventions must address metabolic functionality rather than taxonomic composition alone, as functional redundancy among bacteria means eliminating one species may simply allow another with similar metabolic characteristics to fill the niche. Several limitations warrant acknowledgment: AMON predictions reflect genetic capacity rather than actual enzyme expression or metabolic flux, requiring future validation through isotope tracing or metatranscriptomics; our focus on two specific bacteria necessarily excludes contributions from other microbiome members; plasma metabolomics captures

only metabolites that cross intestinal barriers and survive hepatic metabolism, potentially missing important gut-localized metabolites; and cross-sectional design precludes causal inference, as we cannot distinguish whether *T. sanguinis's* metabolic profile drives fibrosis or whether fibrotic environments select for this metabolic phenotype. Longitudinal studies tracking metabolic changes during disease progression and experimental interventions using gnotobiotic models are needed to establish causality.

Thus, multi-cohort probing of candidate biosignatures, through integrated analyses of multi-omics profiles provide superior insights for potential biomarker development and targeted therapies, specifically for gut microbial determinants of schistosomiasis in our present study (Figure S5).

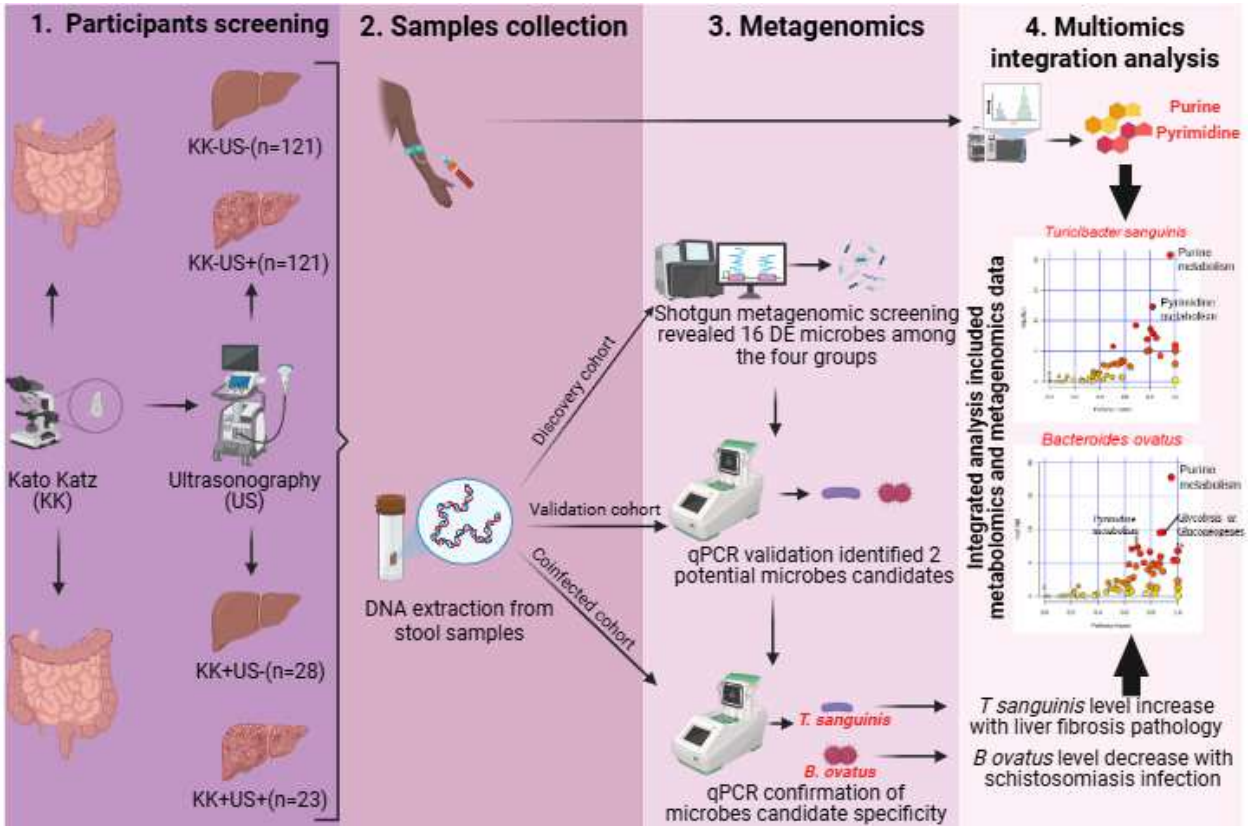


Figure S5: Overview of the human study workflow. **(1)** School-aged children were recruited, screened,

and clustered based on *S. mansoni* infection and liver pathology. **(2)** Stool DNA was extracted for metagenomic analysis and plasma sample for metabolomics profiling. **(3)** Shotgun metagenomic sequencing and bioinformatics analysis identified gut microbial candidates, which were validated by species-specific qPCR quantification in independent cohort and tested for specificity against other infections. **(4)** Multi-omics integration refined organism-specific metabolic interactions between host and microbiome.

Taken together, a conclusive case, through validation of the above 3 canonical postulates on preclinical causality, further tested through association and mechanistic studies in clinical settings, is therefore provided in this study, to unprecedentedly demonstrate the core regulation of schistosomiasis by the host gut microbiome.

CONCLUSION

This study establishes the gut microbiome as a functional regulator of host susceptibility and morbidity during chronic schistosomiasis. Using genetically distinct murine models, we show that fecal microbiota transfer from resistant to susceptible hosts mitigates pathological features and prolongs survival, underscoring the functional role of microbial communities in shaping host responses. In humans, shotgun metagenomics and targeted qPCR analyses identified consistent microbiome alterations associated with *Schistosoma mansoni* infection and morbidity. Notably, *Bacteroides ovatus* emerged as a negative biomarker of infection, while *Turicibacter sanguinis* was positively associated with liver fibrosis. Multi-omics integration linked these taxa to altered purine metabolism and

signaling pathways, highlighting mechanistic connections between microbial activity and parasite biology. These findings highlight the translational potential of microbiome-based biomarkers for monitoring schistosomiasis outcomes in endemic populations.

LIST OF ABBREVIATIONS

AMON – Annotation of Metabolite Origins via Networks

ANOVA – Analysis of Variance

AUC – Area Under the Curve

BacMet - Antibacterial Biocide and Metal Resistance Genes database

BMI – Body Mass Index

BLASTN – Basic Local Alignment Search Tool (Nucleotide)

BSL2 - Biosafety level 2

CAB – Chromotrope Aniline Blue

CAZy – Carbohydrate-Active enZYmes database

CBIO - Cape Town Computational Biology Hub

CDO1 – Cysteine Dioxygenase 1

CH – Co-housing

CIDRI-Africa – Wellcome Centre for Infectious Diseases Research in Africa

CFA – Complete Freund's Adjuvant

CFA – Carbohydrate-Active enZYmes database

COG – Clusters of Orthologous Groups

Da – Dalton

DNA – Deoxyribonucleic Acid

eggNOG – Evolutionary Genealogy of Genes: Non-supervised Orthologous Groups

FC – Fold Change

FMT – Fecal Microbiota Transfer

FXR – Farnesoid X Receptor

GABA – Gamma-Aminobutyric Acid

GSH – Glutathione

H&E – Hematoxylin and Eosin

HMDB – Human Metabolome Database

KEGG – Kyoto Encyclopedia of Genes and Genomes

KK – Kato Katz

LC/MS – Liquid Chromatography / Mass Spectrometry

LDA – Linear Discriminant Analysis

LefSe – Linear Discriminant Analysis Effect Size

MS/MS – Tandem Mass Spectrometry

MSA - Multiple Sequence Alignment

NBRC – National BioResource Project

NCBI – National Center for Biotechnology Information

NR – Non-Redundant (protein database)

OVA – Ovalbumin

PCoA – Principal Coordinates Analysis

PCA – Principal Component Analysis

PiMP – Polyomics Integrated Metabolomics Pipeline

PLS-DA – Partial Least Squares Discriminant Analysis

PPF – Periportal Fibrosis

PZQ – Praziquantel

qPCR – Quantitative Polymerase Chain Reaction

rRNA – Ribosomal RNA

ROC – Receiver Operating Characteristic

SAC – School-Aged Children

SANS – South African National Standard

SAVC – South African Veterinary Council

SCFA – Short-Chain Fatty Acids

SD – Standard Deviation

SPF – Specific Pathogen Free

SREBP1c – Sterol Regulatory Element-Binding Protein 1c

STH – Soil-Transmitted Helminths

TGR5 – Takeda G Protein-Coupled Receptor 5

UPLC – Ultra-Performance Liquid Chromatography

US – Ultrasonography

VIP – Variable Importance in Projection

YAMP – Yet Another Metagenomic Pipeline

SUPPLEMENTARY INFORMATION

Supplementary tables

Table S1: Characteristics of the selected participants for the discovery phase by whole genome shotgun metagenomics sequencing.

Table S2: Characteristics of the selected participants for the validation phase by species-specific real-time quantitative PCR.

Table S3: Microbial species-specific primers used for qPCR-based quantification of the candidate microbes in stool DNA samples for validation.

Table S4: *B. ovatus* pathway analysis showing the top 10 enriched pathways

Table S5: *T: sanguinis* pathway analysis showing the top 10 enriched pathways

Supplementary figures

Figure S1. Workflow for cross-cohort integration analysis of fecal metagenomics and plasma metabolomics in *S. mansoni* infected SAC

Figure S2. qPCR-based validation of candidate biomarking gut microbes on a second cohort of SAC.

Figure S3. Plasma metabolite changes during schistosomiasis

Figure S4. Venn Diagram illustrating overlaps in compound sets following AMON analysis.

Figure S5. Overview of the human study workflow

Supplementary Materials

Supplementary Material 1: Clinical data of school-aged children form discovery cohort.

Supplementary Material 2: Clinical data of school-aged children form validation cohort.

Supplementary Material 3: Abundance of *T. sanguinis* and *B. ovatus* in stool sample of school-aged children from the validation cohort.

Supplementary Material 4: Plasma metabolomics data of school-aged children from discovery cohort (Infection).

Supplementary Material 5: Plasma metabolomics data of school-aged children from discovery cohort (Pathology).

Supplementary Material 6: Pathway analysis of plasma metabolites associated with *Bacteroides ovatus* in *S. mansoni* infection.

Supplementary Material 7: Pathway analysis of plasma metabolites associated with *Turicibacter sanguinis* in *S. mansoni*-related liver fibrosis.

FUNDING STATEMENT

This project is part of the EDCTP2 program supported by the European Union, through grant number TMA2016CDF-1571, with support from grant FLR\R1\191058 of the FLAIR Fellowship Program, a partnership between the African Academy of Sciences and the Royal Society funded by the UK Government's Global Challenges Research Fund to JKN and a Grant from Merck KGaA (Darmstadt, Germany) to JKN. TM was a recipient of a Ph.D. fellowship from the South African National Research Foundation (NRF). MGO, LMK, LJMN, MW and BMZB were receiving fellowships through funds from Merck KGaA during the study. SDK was a former recipient of a PhD fellowship from the International Centre for Genetic Engineering and Biotechnology (ICGEB), Cape Town component, and

a Postdoctoral fellow within a UK Royal Society FLAIR-funded grant (FLR\R1\191058) at the time of the present work. FB was funded by the International Centre for Genetic Engineering and Biotechnology, Cape Town component; the South African National Research Foundation and Medical Research Council with further support from CIDRI-Africa (grant No 203135/Z/16/Z). The funders had no role in study design, data collection and analysis, decision to publish, or preparation of the manuscript.

AUTHOR'S CONTRIBUTIONS

JKN designed the project, the conceptual ideas. Experiment were performed by JKN, TM, MGO, LMK, LJMN, MW, BMZB, VOA, SDK, PM, NAA, DDN, FM, EMK, FK, GKT, FN, AO, RGE, MK, MCOA, KL, CD-G, TS. Data curation and analysis were performed by JKN, TM, MGO, LMK, LJMT, MW, BMZB, VOA, SDK, PM, NAA, DDN, FM, KL, CD-G, TS and FB. JKN, TM, SDK, KL, DDN and FM validated and JKN, TM, MGO, LMK, LJMN, MW, BMZB, VOA, SDK and KL visualized data. Original draft was written by TM, MGO, LMK, CD-G, TS and JKN, while the revision and edition were performed by JKN, TM, MGO, LMK, LJMN, MW, BMZB, VOA, SDK, PM, NAA, DDN, FM, EMK, FK, GKT, FN, AO, RGE, MK, MCOA, KL, CD-G, TS and FB. Funding were acquired by JKN, FB, CD-G, TS and the project was administrated by JKN, CD-G and TS.

ACKNOWLEDGEMENT

We are very grateful to all children who participated in this survey, their parents/authorized legal guardians, the Directors and teachers of the primary schools surveyed. Special gratification to all authorities who granted us with required authorization. We also acknowledge the National Public Health Laboratory of the Ministry of Public Health in Yaoundé, Cameroon where some preliminary analyses were performed. Special thanks are finally due to the National Program for the Control of Schistosomiasis and Soil transmitted Helminthiasis through the Ministry of Public Health and the Ministry of Basic Education of Cameroon for the relentless effort in regularly treating schoolchildren in Cameroon. We are grateful to the University of Cape Town Animal Unit staff for the maintenance of mice. The Ilifu cloud computing facility, Cape Town, South Africa (https://www.ilifu.ac.za/)". We also thank Ms Munadia Ansarie and Mr Jabu Magagula for their valuable technical assistance with animal breeding and Ms Lizette Fick for histology. We do finally acknowledge the critical support of the University of cape Town Computational Biology Group under Prof Nicky Mulder in performing the bioinformatics analyses on the data generated under this project.

DATA AVAILABILITY

Raw sequencing reads from shotgun metagenomics of stool samples collected from school-aged children have been deposited in the NCBI Sequence Read Archive (SRA) under BioProject accession number PRJNA1422631 (https://www.ncbi.nlm.nih.gov/bioproject/1422631;https://www.ncbi.nlm.nih.gov/biosample?LinkName=bioproject_biosample_all&from_uid=1422631). Metagenomic analyses

were conducted using the Nextflow-based pipeline YAMP, available on GitHub (https://github.com/kviljoen/YAMP).

Plasma metabolomics data used in this study are available at the NIH Common Fund's National Metabolomics Data Repository (NMDR) website, the Metabolomics Workbench [82] under the project PR003034 (http://dx.doi.org/10.21228/M8H56J). The analysis source code supporting the findings of this study is openly accessible at GitHub (https://gist.github.com/kviljoen/97d36c689c5c9b9c39939c7a100720b9).

All R scripts employed for downstream statistical analyses are openly accessible at https://gist.github.com/kviljoen/97d36c689c5c9b9c39939c7a100720b9.

REFERENCES

1. McManus DP, Dunne DW, Sacko M, Utzinger J, Vennervald BJ, Zhou XN: **Schistosomiasis**. *Nat Rev Dis Primers* 2018, **4:**13.
2. Mawa PA, Kincaid-Smith J, Tukahebwa EM, Webster JP, Wilson S: **Schistosomiasis Morbidity Hotspots: Roles of the Human Host, the Parasite and Their Interface in the Development of Severe Morbidity**. *Front Immunol* 2021, **12:**635869.
3. Steinmann P, Keiser J, Bos R, Tanner M, Utzinger J: **Schistosomiasis and water resources development: systematic review, meta-analysis, and estimates of people at risk**. *Lancet Infect Dis* 2006, **6:**411-425.
4. Hams E, Aviello G, Fallon PG: **The schistosoma granuloma: friend or foe?** *Front Immunol* 2013, **4:**89.
5. Schwartz C, Fallon PG: **Schistosoma "Eggs-lting" the Host: Granuloma Formation and Egg Excretion**. *Front Immunol* 2018, **9:**2492.
6. Taylor JJ, Krawczyk CM, Mohrs M, Pearce EJ: **Th2 cell hyporesponsiveness during chronic murine schistosomiasis is cell intrinsic and linked to GRAIL expression**. *J Clin Invest* 2009, **119:**1019-1028.
7. Turner JD, Jenkins GR, Hogg KG, Aynsley SA, Paveley RA, Cook PC, Coles MC, Mountford AP: **CD4+CD25+ regulatory cells contribute to the regulation**

of colonic Th2 granulomatous pathology caused by schistosome infection. *PLoS Negl Trop Dis* 2011, **5:**e1269.

8. Wiegand RE, Fleming FM, de Vlas SJ, Odiere MR, Kinung'hi S, King CH, Evans D, French MD, Montgomery SP, Straily A, Utzinger J, Vounatsou P, Secor WE: **Defining elimination as a public health problem for schistosomiasis control programmes: beyond prevalence of heavy-intensity infections**. *Lancet Glob Health* 2022, **10:**e1355-e1359.

9. Nono JK, Fu K, Mpotje T, Varrone G, Aziz NA, Mosala P, Hlaka L, Kamdem SD, Xu D, Spangenberg T, Brombacher F: **Investigating the antifibrotic effect of the antiparasitic drug Praziquantel in in vitro and in vivo preclinical models**. *Sci Rep* 2020, **10:**10638.

10. Molloy MJ, Bouladoux N, Belkaid Y: **Intestinal microbiota: shaping local and systemic immune responses**. *Semin Immunol* 2012, **24:**58-66.

11. Holzscheiter M, Layland LE, Loffredo-Verde E, Mair K, Vogelmann R, Langer R, Wagner H, Prazeres da CC: **Lack of host gut microbiota alters immune responses and intestinal granuloma formation during schistosomiasis**. *Clin Exp Immunol* 2014, **175:**246-257.

12. Osakunor DNM, Munk P, Mduluza T, Petersen TN, Brinch C, Ivens A, Chimponda T, Amanfo SA, Murray J, Woolhouse MEJ, Aarestrup FM, Mutapi F: **The gut microbiome but not the resistome is associated with urogenital schistosomiasis in preschool-aged children**. *Commun Biol* 2020, **3:**155.

13. Jiang Y, Yuan Z, Shen Y, Rosa BA, Martin J, Cao S, Zhou Y, Mitreva M, Cao J: **Alteration of the fecal microbiota in Chinese patients with Schistosoma japonicum infection**. *Parasite* 2021, **28:**1.

14. Afful P, Abotsi GK, Adu-Gyamfi CO, Benyem G, Katawa G, Kyei S, Arndts K, Ritter M, Asare KK: **Schistosomiasis-Microbiota Interactions: A Systematic Review and Meta-Analysis**. *Pathogens* 2024, **13**.

15. Oyono MG, Kenmoe S, Ebogo Belobo JT, Mbah Ntepe LJ, Kameni M, Kamguia LM, Mpotje T, Nono JK: **Diagnostic, prognostic, and therapeutic potentials of gut microbiome profiling in human schistosomiasis: A comprehensive systematic review**. *PLoS Negl Trop Dis* 2025, **19:**e0012844.

16. Stark KA, Rinaldi G, Costain A, Clare S, Tolley C, Almeida A, McCarthy C, Harcourt K, Brandt C, Lawley TD, Berriman M, MacDonald AS, Forde-Thomas JE, Hulme BJ, Hoffmann KF, Cantacessi C, Cortes A: **Gut microbiota and immune profiling of microbiota-humanised versus wildtype mouse models of hepatointestinal schistosomiasis**. *Anim Microbiome* 2024, **6:**36.

17. Caruso R, Ono M, Bunker ME, Nunez G, Inohara N: **Dynamic and Asymmetric Changes of the Microbial Communities after Cohousing in Laboratory Mice**. *Cell Rep* 2019, **27:**3401-3412.

18. Kamdem SD, Konhawa F, Kuemkon EM, Meyo KL, Tchanana GK, Nche F, Oumarou A, Hamza M, Ouratou Y, Tcheutchoua MN, Ghislain ER, Ngogang MP, Kengne M, Netongo PM, Ondigui BE, Okomo Assoumou MC, Brombacher F, Nono JK: **Negative Association of Interleukin-33 Plasma Levels and Schistosomiasis Infection in a Site of Polyparasitism in Rural Cameroon**. *Front Immunol* 2019, **10:**2827.

19. Segata N, Izard J, Waldron L, Gevers D, Miropolsky L, Garrett WS, Huttenhower C: **Metagenomic biomarker discovery and explanation**. *Genome Biol* 2011, **12:**R60.

20. Truong DT, Franzosa EA, Tickle TL, Scholz M, Weingart G, Pasolli E, Tett A, Huttenhower C, Segata N: **MetaPhlAn2 for enhanced metagenomic taxonomic profiling**. *Nat Methods* 2015, **12:**902-903.

21. Visconti A, Martin TC, Falchi M: **YAMP: a containerized workflow enabling reproducibility in metagenomics research**. *Gigascience* 2018, **7**.

22. McMurdie PJ, Holmes S: **phyloseq: an R package for reproducible interactive analysis and graphics of microbiome census data**. *PLoS One* 2013, **8:**e61217.

23. Wickham H: *ggplot2: Elegant Graphics for Data Analysis.* New York: Springer-Verlag; 2016.

24. Shaffer M, Thurimella K, Quinn K, Doenges K, Zhang X, Bokatzian S, Reisdorph N, Lozupone CA: **AMON: annotation of metabolite origins via networks to integrate microbiome and metabolome data**. *BMC Bioinformatics* 2019, **20:**614.

25. Abdel AN, Berkiks I, Mosala P, Brombacher TM, Brombacher F: **Environmental and microbial factors influence affective and cognitive behavior in C57BL/6 sub-strains**. *Front Immunol* 2023, **14:**1139913.

26. World Health Organization: *Ultrasound in schistosomiasis : a practical guide to the standard use of ultrasonography for assessment of schistosomiasis-related morbidity*: World Health Organization; 2000.

27. Clifford RJ, Milillo M, Prestwood J, Quintero R, Zurawski DV, Kwak YI, Waterman PE, Lesho EP, Mc GP: **Detection of bacterial 16S rRNA and identification of four clinically important bacteria by real-time PCR**. *PLoS One* 2012, **7:**e48558.

28. Duvallet C, Gibbons SM, Gurry T, Irizarry RA, Alm EJ: **Meta-analysis of gut microbiome studies identifies disease-specific and shared responses**. *Nat Commun* 2017, **8:**1784.

29. Keshet A, Segal E: **Identification of gut microbiome features associated with host metabolic health in a large population-based cohort**. *Nat Commun* 2024, **15:**9358.

30. Stark KA, Rinaldi G, Cortes A, Costain A, MacDonald AS, Cantacessi C: **The role of the host gut microbiome in the pathophysiology of schistosomiasis**. *Parasite Immunol* 2023, **45:**e12970.

31. Mutapi F: **The gut microbiome in the helminth infected host**. *Trends Parasitol* 2015, **31:**405-406.

32. Cortes A, Peachey LE, Jenkins TP, Scotti R, Cantacessi C: **Helminths and microbes within the vertebrate gut - not all studies are created equal**. *Parasitology* 2019, **146:**1371-1378.

33. Neville BA, Forster SC, Lawley TD: **Commensal Koch's postulates: establishing causation in human microbiota research**. *Curr Opin Microbiol* 2018, **42:**47-52.

34. Robertson SJ, Lemire P, Maughan H, Goethel A, Turpin W, Bedrani L, Guttman DS, Croitoru K, Girardin SE, Philpott DJ: **Comparison of Co-housing and Littermate Methods for Microbiota Standardization in Mouse Models**. *Cell Rep* 2019, **27:**1910-1919.

35. Hong Y, Sheng L, Zhong J, Tao X, Zhu W, Ma J, Yan J, Zhao A, Zheng X, Wu G, Li B, Han B, Ding K, Zheng N, Jia W, Li H: **Desulfovibrio vulgaris, a potent acetic acid-producing bacterium, attenuates nonalcoholic fatty liver disease in mice**. *Gut Microbes* 2021, **13:**1-20.

36. Vannella KM, Barron L, Borthwick LA, Kindrachuk KN, Narasimhan PB, Hart KM, Thompson RW, White S, Cheever AW, Ramalingam TR, Wynn TA: **Incomplete deletion of IL-4Ralpha by LysM(Cre) reveals distinct subsets of M2 macrophages controlling inflammation and fibrosis in chronic schistosomiasis**. *PLoS Pathog* 2014, **10:**e1004372.

37. Herbert DR, Holscher C, Mohrs M, Arendse B, Schwegmann A, Radwanska M, Leeto M, Kirsch R, Hall P, Mossmann H, Claussen B, Forster I, Brombacher F: **Alternative macrophage activation is essential for survival during schistosomiasis and downmodulates T helper 1 responses and immunopathology**. *Immunity* 2004, **20:**623-635.

38. Metwaly A, Kriaa A, Hassani Z, Carraturo F, Druart C, Arnauts K, Wilmes P, Walter J, Rosshart S, Desai MS, Dore J, Fasano A, Blottiere HM, Maguin E, Haller D: **A Consensus Statement on establishing causality, therapeutic**

applications and the use of preclinical models in microbiome research. *Nat Rev Gastroenterol Hepatol* 2025, **22:**343-356.

39. Sanna S, van Zuydam NR, Mahajan A, Kurilshikov A, Vich VA, Vosa U, Mujagic Z, Masclee AAM, Jonkers DMAE, Oosting M, Joosten LAB, Netea MG, Franke L, Zhernakova A, Fu J, Wijmenga C, McCarthy MI: **Causal relationships among the gut microbiome, short-chain fatty acids and metabolic diseases**. *Nat Genet* 2019, **51:**600-605.

40. Zhang Y, Huang A, Li J, Munthali W, Cao S, Putri UMP, Yang L: **The Effect of Microbiome-Modulating Agents (MMAs) on Type 1 Diabetes: A Systematic Review and Meta-Analysis of Randomized Controlled Trials**. *Nutrients* 2024, **16**.

41. Liang W, Enee E, Andre-Vallee C, Falcone M, Sun J, Diana J: **Intestinal Cathelicidin Antimicrobial Peptide Shapes a Protective Neonatal Gut Microbiota Against Pancreatic Autoimmunity**. *Gastroenterology* 2022, **162:**1288-1302.

42. Huang S, Li F, Quan C, Jin D: **Intestinal flora: a potential pathogenesis mechanism and treatment strategy for type 1 diabetes mellitus**. *Gut Microbes* 2024, **16:**2423024.

43. Nirmalkar K, Qureshi F, Kang DW, Hahn J, Adams JB, Krajmalnik-Brown R: **Shotgun Metagenomics Study Suggests Alteration in Sulfur Metabolism and Oxidative Stress in Children with Autism and Improvement after Microbiota Transfer Therapy**. *Int J Mol Sci* 2022, **23**.

44. Kang DW, Adams JB, Gregory AC, Borody T, Chittick L, Fasano A, Khoruts A, Geis E, Maldonado J, McDonough-Means S, Pollard EL, Roux S, Sadowsky MJ, Lipson KS, Sullivan MB, Caporaso JG, Krajmalnik-Brown R: **Microbiota Transfer Therapy alters gut ecosystem and improves gastrointestinal and autism symptoms: an open-label study**. *Microbiome* 2017, **5:**10.

45. Takyi E, Nirmalkar K, Adams J, Krajmalnik-Brown R: **Interventions targeting the gut microbiota and their possible effect on gastrointestinal and neurobehavioral symptoms in autism spectrum disorder**. *Gut Microbes* 2025, **17:**2499580.

46. Tuttle AH, Philip VM, Chesler EJ, Mogil JS: **Comparing phenotypic variation between inbred and outbred mice**. *Nat Methods* 2018, **15:**994-996.

47. Jayasinghe S, Byrne NM, Hills AP: **Cultural influences on dietary choices**. *Prog Cardiovasc Dis* 2025.

48. Buonfrate D, Ferrari TCA, Adegnika AA, Russell SJ, Gobbi FG: **Human schistosomiasis**. *Lancet* 2025, **405:**658-670.

49. Horvath TD, Ihekweazu FD, Haidacher SJ, Ruan W, Engevik KA, Fultz R, Hoch KM, Luna RA, Oezguen N, Spinler JK, Haag AM, Versalovic J, Engevik MA: **Bacteroides ovatus colonization influences the abundance of intestinal short chain fatty acids and neurotransmitters**. *iScience* 2022, **25:**104158.

50. Fahmy AM, William S, Hegab A, Tm D: **Schistosomicidal and hepatoprotective activity of gamma-aminobutyric acid (GABA) alone or combined with praziquantel against Schistosoma mansoni infection in murine model**. *Exp Parasitol* 2022, **238:**108260.

51. Lynch JB, Gonzalez EL, Choy K, Faull KF, Jewell T, Arellano A, Liang J, Yu KB, Paramo J, Hsiao EY: **Gut microbiota Turicibacter strains differentially modify bile acids and host lipids**. *Nat Commun* 2023, **14:**3669.

52. Kwan SY, Jiao J, Qi J, Wang Y, Wei P, McCormick JB, Fisher-Hoch SP, Beretta L: **Bile Acid Changes Associated With Liver Fibrosis and Steatosis in the Mexican-American Population of South Texas**. *Hepatol Commun* 2020, **4:**555-568.

53. Saga K, Iwashita Y, Hidano S, Aso Y, Isaka K, Kido Y, Tada K, Takayama H, Masuda T, Hirashita T, Endo Y, Ohta M, Kobayashi T, Inomata M: **Secondary Unconjugated Bile Acids Induce Hepatic Stellate Cell Activation**. *Int J Mol Sci* 2018, **19**.

54. Mars RAT, Yang Y, Ward T, Houtti M, Priya S, Lekatz HR, Tang X, Sun Z, Kalari KR, Korem T, Bhattarai Y, Zheng T, Bar N, Frost G, Johnson AJ, Van TW, Han S, Ordog T, Grover M, Sonnenburg J, D'Amato M, Camilleri M, Elinav E, Segal E, Blekhman R, Farrugia G, Swann JR, Knights D, Kashyap PC: **Longitudinal Multi-omics Reveals Subset-Specific Mechanisms Underlying Irritable Bowel Syndrome**. *Cell* 2020, **183:**1137-1140.

55. Lee JS, Wang RX, Alexeev EE, Lanis JM, Battista KD, Glover LE, Colgan SP: **Hypoxanthine is a checkpoint stress metabolite in colonic epithelial energy modulation and barrier function**. *J Biol Chem* 2018, **293:**6039-6051.

56. Ornelas A, Dowdell AS, Lee JS, Colgan SP: **Microbial Metabolite Regulation of Epithelial Cell-Cell Interactions and Barrier Function**. *Cells* 2022, **11**.

57. Ahmed SF, Oswald IP, Caspar P, Hieny S, Keefer L, Sher A, James SL: **Developmental differences determine larval susceptibility to nitric oxide-mediated killing in a murine model of vaccination against Schistosoma mansoni**. *Infect Immun* 1997, **65:**219-226.

58. Shen J, Lai DH, Wilson RA, Chen YF, Wang LF, Yu ZL, Li MY, He P, Hide G, Sun X, Yang TB, Wu ZD, Ayala FJ, Lun ZR: **Nitric oxide blocks the**

development of the human parasite Schistosoma japonicum. *Proc Natl Acad Sci U S A* 2017, **114:**10214-10219.

59. Zhou S, Lu Y, Chen J, Pan Z, Pang L, Wang Y, Zhang Q, Strand MR, Chen XX, Huang J: **Parasite reliance on its host gut microbiota for nutrition and survival**. *ISME J* 2022, **16:**2574-2586.

60. Drew GC, Stevens EJ, King KC: **Microbial evolution and transitions along the parasite-mutualist continuum**. *Nat Rev Microbiol* 2021, **19:**623-638.

61. Kobel CM, Merkesvik J, Burgos IMT, Lai W, Oyas O, Pope PB, Hvidsten TR, Aho VTE: **Integrating host and microbiome biology using holo-omics**. *Mol Omics* 2024, **20:**438-452.

62. Srinak N, Kruger F, Kaleta C, Taubenheim J: **Metabolic modeling of host-microbe interactions**. *Comput Struct Biotechnol J* 2025, **27:**4304-4319.

63. Li T, Hasan MN, Gu L: **Bile acids regulation of cellular stress responses in liver physiology and diseases**. *eGastroenterology* 2024, **2**.

64. Miyazaki T, Ueda H, Ikegami T, Honda A: **Upregulation of Taurine Biosynthesis and Bile Acid Conjugation with Taurine through FXR in a Mouse Model with Human-like Bile Acid Composition**. *Metabolites* 2023, **13**.

65. Wang Y, Li J, Matye D, Zhang Y, Dennis K, Ding WX, Li T: **Bile acids regulate cysteine catabolism and glutathione regeneration to modulate hepatic sensitivity to oxidative injury**. *JCI Insight* 2018, **3**.

66. Ali RO, Haddad JA, Quinn GM, Zhang GY, Townsend E, Scheuing L, Hill KL, Menkart M, Oringher JL, Umarova R, Rampertaap S, Rosenzweig SD, Koh C, Levy EB, Kleiner DE, Etzion O, Heller T: **Taurine-conjugated bile acids and their link to hepatic S1PR2 play a significant role in hepatitis C-related liver disease**. *Hepatol Commun* 2024, **8**.

67. Zhang B, Li J, Zong X, Wang J, Xin L, Song H, Zhang W, Koda S, Hua H, Zhang B, Yu Q, Zheng KY, Yan C: **FXR deficiency in hepatocytes disrupts the bile acid homeostasis and inhibits autophagy to promote liver injury in Schistosoma japonicum-infected mice**. *PLoS Negl Trop Dis* 2022, **16:**e0010651.

68. Anderson ME: **Glutathione: an overview of biosynthesis and modulation**. *Chem Biol Interact* 1998, **111-112:**1-14.

69. de Oliveira RB, Senger MR, Vasques LM, Gasparotto J, dos Santos JP, Pasquali MA, Moreira JC, Silva FP, Jr., Gelain DP: **Schistosoma mansoni infection causes oxidative stress and alters receptor for advanced glycation endproduct (RAGE) and tau levels in multiple organs in mice**. *Int J Parasitol* 2013, **43:**371-379.

70. Brandsch C, Schmidt T, Behn D, Weisse K, Mueller AS, Stangl GI: **Glutathione deficiency down-regulates hepatic lipogenesis in rats**. *Lipids Health Dis* 2010, **9:**50.

71. Tsuchida T, Friedman SL: **Mechanisms of hepatic stellate cell activation**. *Nat Rev Gastroenterol Hepatol* 2017, **14:**397-411.

72. Schon HT, Bartneck M, Borkham-Kamphorst E, Nattermann J, Lammers T, Tacke F, Weiskirchen R: **Pharmacological Intervention in Hepatic Stellate Cell Activation and Hepatic Fibrosis**. *Front Pharmacol* 2016, **7:**33.

73. Ariyaratne A, Finney CAM: **Eosinophils and Macrophages within the Th2-Induced Granuloma: Balancing Killing and Healing in a Tight Space**. *Infect Immun* 2019, **87**.

74. Grondin JA, Jamal A, Mowna S, Seto T, Khan WI: **Interaction between Intestinal Parasites and the Gut Microbiota: Implications for the Intestinal Immune Response and Host Defence**. *Pathogens* 2024, **13**.

75. Helmby H, Hafalla JC: **Parasites and tissue microenvironment**. *Parasite Immunol* 2021, **43:**e12810.

76. Saveljeva S, Sewell GW, Ramshorn K, Cader MZ, West JA, Clare S, Haag LM, de Almeida Rodrigues RP, Unger LW, Iglesias-Romero AB, Holland LM, Bourges C, Md-Ibrahim MN, Jones JO, Blumberg RS, Lee JC, Kaneider NC, Lawley TD, Bradley A, Dougan G, Kaser A: **A purine metabolic checkpoint that prevents autoimmunity and autoinflammation**. *Cell Metab* 2022, **34:**106-124.

77. Jain S, Jacobson KA: **Purinergic Signaling in Liver Pathophysiology**. *Front Endocrinol (Lausanne)* 2021, **12:**718429.

78. Velazquez-Miranda E, Diaz-Munoz M, Vazquez-Cuevas FG: **Purinergic signaling in hepatic disease**. *Purinergic Signal* 2019, **15:**477-489.

79. Xiong Y, Wu L, Shao L, Wang Y, Huang Z, Huang X, Li C, Wu A, Liu Z, Fan X, Zhou P: **Dynamic Alterations of the Gut Microbial Pyrimidine and Purine Metabolism in the Development of Liver Cirrhosis**. *Front Mol Biosci* 2021, **8:**811399.

80. Sawitza I, Kordes C, Gotze S, Herebian D, Haussinger D: **Bile acids induce hepatic differentiation of mesenchymal stem cells**. *Sci Rep* 2015, **5:**13320.

81. Chiang JYL, Ferrell JM: **Bile acid receptors FXR and TGR5 signaling in fatty liver diseases and therapy**. *Am J Physiol Gastrointest Liver Physiol* 2020, **318:**G554-G573.

82. Sud M, Fahy E, Cotter D, Azam K, Vadivelu I, Burant C, Edison A, Fiehn O, Higashi R, Nair KS, Sumner S, Subramaniam S: **Metabolomics Workbench: An international repository for metabolomics data and metadata, metabolite standards, protocols, tutorials and training, and analysis tools**. *Nucleic Acids Res* 2016, **44:**D463-D470.

Supplementary Files

This is a list of supplementary files associated with this preprint. Click to download.

- SM1Clinicaldataofschoolagedchildrenformdiscoverycohort.docx
- SM2Clinicaldataofschoolagedchildrenformvalidationcohort.docx
- SM3AbundanceofT.sanguinisandB.ovatusinstoolsampleofschoolagedchildrenfromthevalidationcohort.docx
- SM7MetabolicpathwaysanalysisofTuricibactersanguinis.docx
- SM6MetabolicpathwaysanalysisofBacteroidesovatus.docx
- SM4Plasmametabolomicsdatafromschoolagedchildrendiscoverycohort Infection.xlsx
- SM5Plasmametabolomicsdatafromschoolagedchildrendiscovery Pathology.xlsx